Sub-Antartic glacier extensions in the Kerguelen region (49° S, Indian Ocean) over the past 24 000 years constrained by 36Cl moraine dating

Vincent Jomelli, Fatima Mokadem, Irene Schimmelpfennig, Emmanuel Chapron, Vincent Rinterknecht, Vincent Favier, Deborah Verfaillie, Daniel Brunstein, Claude Legentil, Elisabeth Michel, et al.

Quaternary Science Reviews 162 (2017) 128–144

Contents lists available at ScienceDirect

Quaternary Science Reviews

journal homepage: www.elsevier.com/locate/quascirev

Sub-Antarctic glacier extensions in the Kerguelen region (49°S, Indian Ocean) over the past 24,000 years constrained by ^{36}Cl moraine dating

Vincent Jomelli [a, *], Fatima Mokadem [a], Irene Schimmelpfennig [b], Emmanuel Chapron [c, d], Vincent Rinterknecht [a], Vincent Favier [e], Deborah Verfaillie [e], Daniel Brunstein [a], Claude Legentil [a], Elisabeth Michel [f], Didier Swingedouw [g], Alain Jaouen [h], Georges Aumaitre [b, i], Didier L. Bourlès [b, i], Karim Keddadouche [b, i]

[a] Université Paris 1 Panthéon-Sorbonne, CNRS Laboratoire de Géographie Physique, 92195 Meudon, France
[b] Aix Marseille Univ, CNRS, IRD, Coll France, CEREGE, Aix-en-Provence, France
[c] Institut des Sciences de la Terre d'Orléans, ISTO, UMR 7327 CNRS-Université d'Orléans-BRGM, Campus Géosciences 1A rue de la Ferolerie, 45071 Orléans Cedex 2, France
[d] Géographie de l'Environnement, GEODE UMR 5602 CNRS Université Toulouse Jean Jaurès, 5 Allée A. Machado, 31058 Toulouse Cedex 9, France
[e] Univ. Grenoble Alpes, LGGE, CNRS, F-38041 Grenoble, France
[f] LSCE, Saclay, Gif sur Yvette 91191, France
[g] UMR CNRS 5805 EPOC – OASU – Université de Bordeaux, Allée Geoffroy St Hilaire, 33615 Pessac, France
[h] Institut Polaire Français Paul-Emile Victor, 29280 Plouzané, France
[i] ASTER Team, France

ARTICLE INFO

Article history:
Received 25 October 2016
Received in revised form
24 January 2017
Accepted 6 March 2017

Keywords:
Glacier fluctuations
^{36}Cl cosmic-ray exposure dating
Late Glacial
Holocene
Kerguelen

ABSTRACT

Similar to many other regions in the world, glaciers in the southern sub-polar regions are currently retreating. In the Kerguelen Islands (49°S, 69°E), the mass balance of the Cook Ice Cap (CIC), the largest ice cap in this region, experienced dramatic shrinking between 1960 and 2013 with retreat rates among the highest in the world. This observation needs to be evaluated in a long-term context. However, data on the past glacier extents are sparse in the sub-Antarctic regions. To investigate the deglaciation pattern since the Last Glacial Maximum (LGM) period, we present the first 13 cosmogenic ^{36}Cl surface exposure ages from four sites in the Kerguelen Islands. The ^{36}Cl ages from erratic and moraine boulders span from 24.4 ± 2.7 ka to 0.3 ± 0.1 ka. We combined these ages with existing glacio-marine radiocarbon ages and bathymetric data to document the temporal and spatial changes of the island's glacial history. Ice began to retreat on the main island before 24.4 ± 2.7 ka until around the time of the Antarctic Cold Reversal (ACR) period (~14.5–12.9 ka), during which the Bontemps moraine was formed by the advance of a CIC outlet glacier. Deglaciation continued during the Holocene probably until 3 ka with evidence of minor advances during the last millennium. This chronology is in pace with major changes in δ^{18}O in a recent West Antarctica ice core record, showing that Kerguelen Islands glaciers are particularly sensitive and relevant to document climate change in the southern polar regions.

1. Introduction

Reconstructing the extent of glaciers in the past and investigating their main climate drivers constitutes a base-line to which the impact of recent climatic changes on glaciers can be compared (Solomina et al., 2015). In the mid-southern latitudes, glaciers are subject to the influence of maritime air masses from different Pacific, Atlantic and Indian ocean origins. Recent investigations on Patagonian and New Zealand glaciers revealed similar patterns of changes since the Late Glacial (19.0–11.6 ka) (Kaplan et al., 2008, 2010; Schaefer et al., 2009, Putnam et al., 2010, 2013a,b; Aniya, 2013; Strelin et al., 2014; Darwill et al., 2016), with for instance a major glacier advance during the Antarctic Cold Reversal (ACR, ~14.5–12.9 ka). However, little is known about glacier fluctuations since the global Last Glacial Maximum (LGM) in the Indian Ocean's sub-Antarctic regions located between Patagonia and New Zealand

* Corresponding author.
E-mail address: vincent.jomelli@lgp.cnrs.fr (V. Jomelli).

http://dx.doi.org/10.1016/j.quascirev.2017.03.010
0277-3791/

(Hodgson et al., 2014a; Solomina et al., 2015). This is due to the scarcity of glacier-covered zones in this area. Rare geochronological constrains have been reported in the South Orkney Islands (60°35′S, 45°30′W), where radiocarbon ages from marine sediment cores revealed ice advances between 13.8 cal ka BP and 9.4 cal ka BP (Bentley et al., 2007). In South Georgia (54°17′S, 36°30′W) (Fig. 1), two onshore moraines were dated by ^{10}Be cosmic-ray exposure (CRE) (Bentley et al., 2007). The resulting ages recalibrated with the southern Hemisphere ^{10}Be production rate (Kaplan et al., 2011) are 16.2 ± 1.8 ^{10}Be ka and 4.6 ± 1.4 ^{10}Be ka, respectively. To our knowledge, except these two locations in the Southern Atlantic, no CRE ages exist for the Southern Pacific or Southern Indian oceans.

The Kerguelen Islands (Fig. 1) are located in the Indian Ocean and represent a unique site because they constitute the largest currently glaciated archipelago (520 km^2 glaciated in 2010; Berthier et al., 2009) with several marine and land terminating margins from the Cook Ice Cap (CIC) (Hodgson et al., 2014a). Hence, constraining the timing of glacier changes in Kerguelen offers a unique opportunity to document glacier fluctuations since the LGM and to investigate the local climate mechanisms responsible for

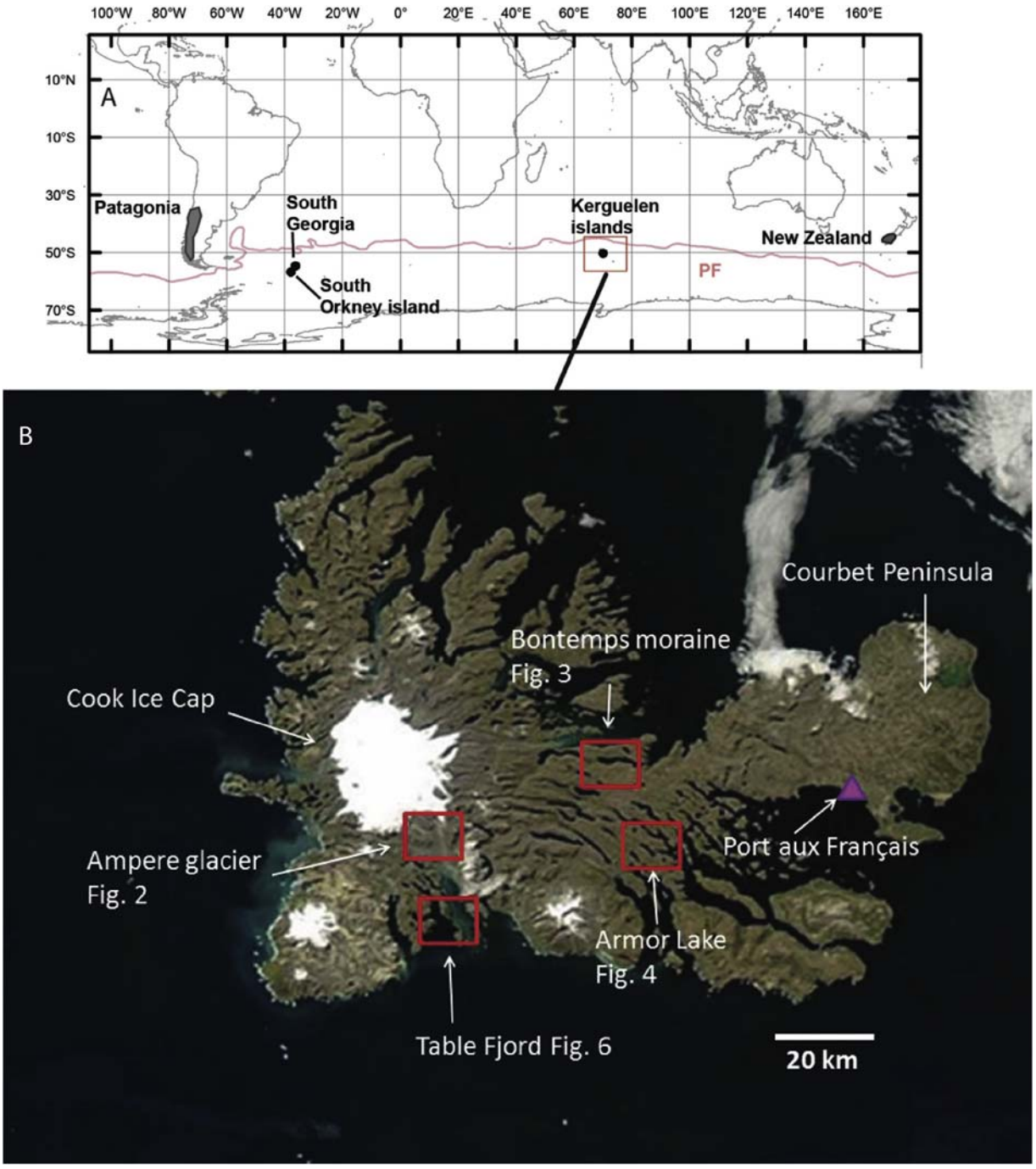

Fig. 1. A, Mid-southern latitude sites discussed in the text and location of the Kerguelen Archipelago. Pink line = polar front after Sallée et al. (2008). Grey surfaces represent the sub-Antarctic ice surface regions discussed in this paper. B, MODIS© image showing sample sites analyzed in this paper with reference to their respective figures. Purple Triangle = Port aux Français research station. (For interpretation of the references to colour in this figure legend, the reader is referred to the web version of this article.)

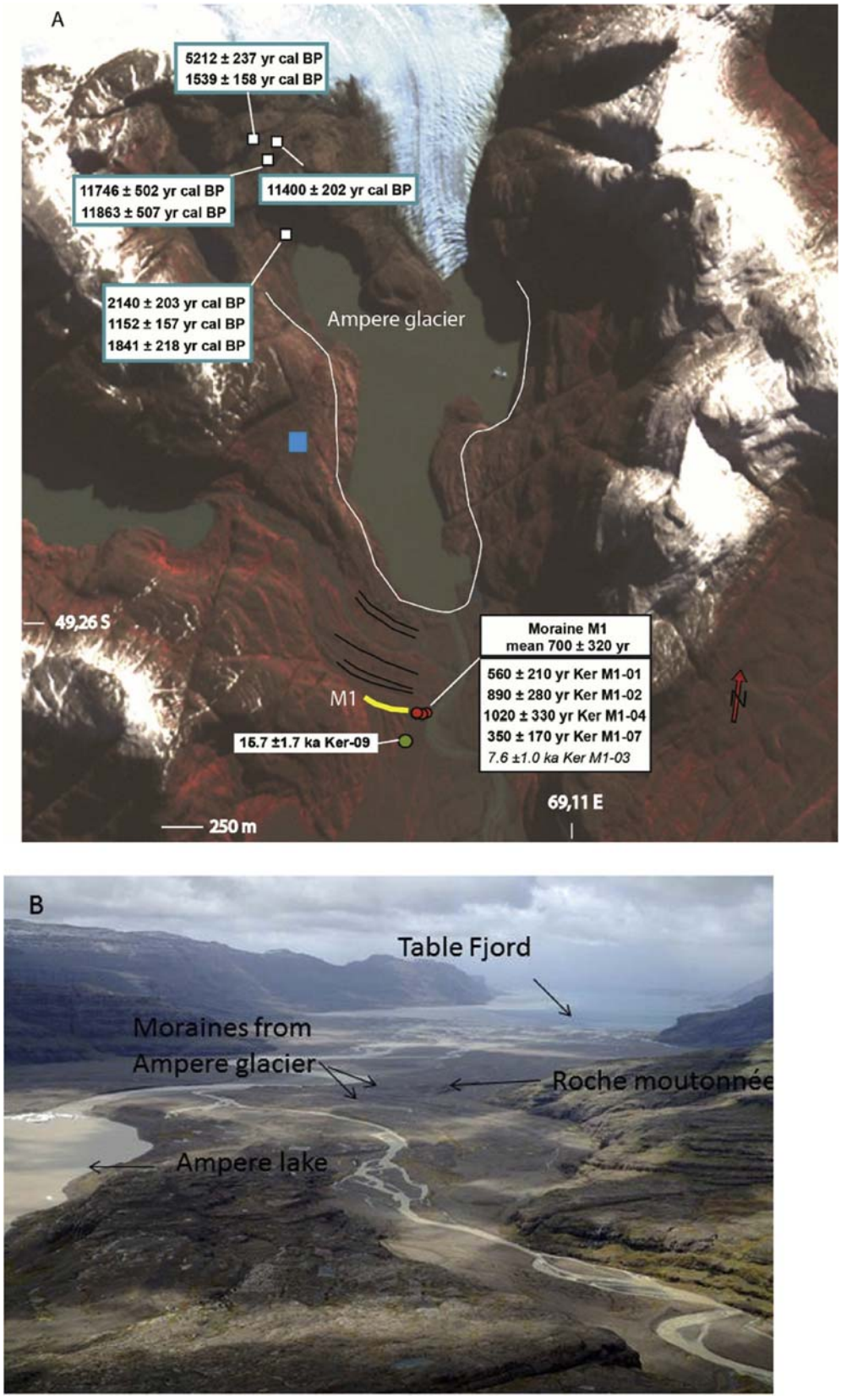

Fig. 2. Ampere Glacier and moraine records. A: Locations of Ampere moraine samples (red dots) and the roche moutonnée sample (green dot) with the corresponding individual ^{36}Cl ages. Also shown is the arithmetic mean age for moraine M1 with the 1σ uncertainty including standard deviation, analytical and production rate uncertainties. Sample Ker M1-03 in italic was rejected as an outlier based on statistical tests. Black lines show moraines that were assigned to the 19–20th centuries by Frenot et al. (1993). White line shows the front position in the 1970s. White squares display calibrated ^{14}C ages from Frenot et al. (1997). The blue square represent the position of shot of the photograph in B; B: Oblique photograph showing the locations of the ^{36}Cl-dated surfaces and Table Fjord in relation to Ampere lake. (For interpretation of the references to colour in this figure legend, the reader is referred to the web version of this article.)

Table 1
Geographic sample locations, topographic shielding factor, and sample thickness.

Sample Name	Latitude (°S)	Longitude (°E)	Elevation (m)	Shielding factor	Thickness (cm)
Ampère moraine M1					
Ker-M1-01	49.44482	69.19164	27	0.995	3
Ker-M1-02	49.44481	69.19131	27	0.997	3
Ker-M1-03	49.44462	69.18935	32	0.977	3
Ker-M1-04	49.44463	69.18935	32	0.984	3
Ker-M1-07	49.44442	69.18886	34	0.989	4
Roche moutonnée					
Ker-09	49.44837	69.18799	25	0.998	4
Erratic boulders on Presqu'ile Bouquet de la Grye					
KBT1	49.28717	69.57753	82	0.996	3
KBT2	49.28967	69.57990	69	0.996	3
Bontemps moraine					
KBT4	49.30237	69.55442	16	0.993	3
KBT5	49.30273	69.55437	16	0.993	3
KBT6	49.30293	69.55487	13	0.993	3
Erratic boulders at Amor lake					
Ker- 23	49.49309	69.71265	177	1.000	3
Ker- 25	49.49391	69.71260	176	1.000	3

possible asynchronies between the Atlantic, Indian and Pacific zones of the sub-Antarctic area.

Here, we present the first direct dating of glacier fluctuations at Kerguelen from 13 ^{36}Cl CRE ages obtained from one roche moutonnée surface, four erratics and eight boulders collected on moraines from two CIC outlet glaciers: Ampere and Explorateur. We combine these ^{36}Cl ages with multibeam bathymetric data and radiocarbon ages from glacio-marine sediment cores collected in the fjord connected to Table Bay draining the Ampere glacier (Fig. 1). These new chronologic data allow us to discuss glacier advances and retreats since the LGM on Kerguelen and compare this chronology with other proxy records from southern Hemisphere.

2. Study area

The French Kerguelen archipelago is a group of 300 isolated islands (Fig. 1). The main island with an area of 7200 km^2 is the largest sub-Antarctic island. The archipelago is an emerged part of the Kerguelen oceanic plateau of volcanic origin dominated by basaltic lava flows and formed about 40 Myr ago. The western part of the archipelago is dominated by a mountainous morphology with numerous U-shaped valleys and fjords. It is mostly covered by the CIC, the largest ice cap on this island (410 km^2 in 2011, Verfaillie

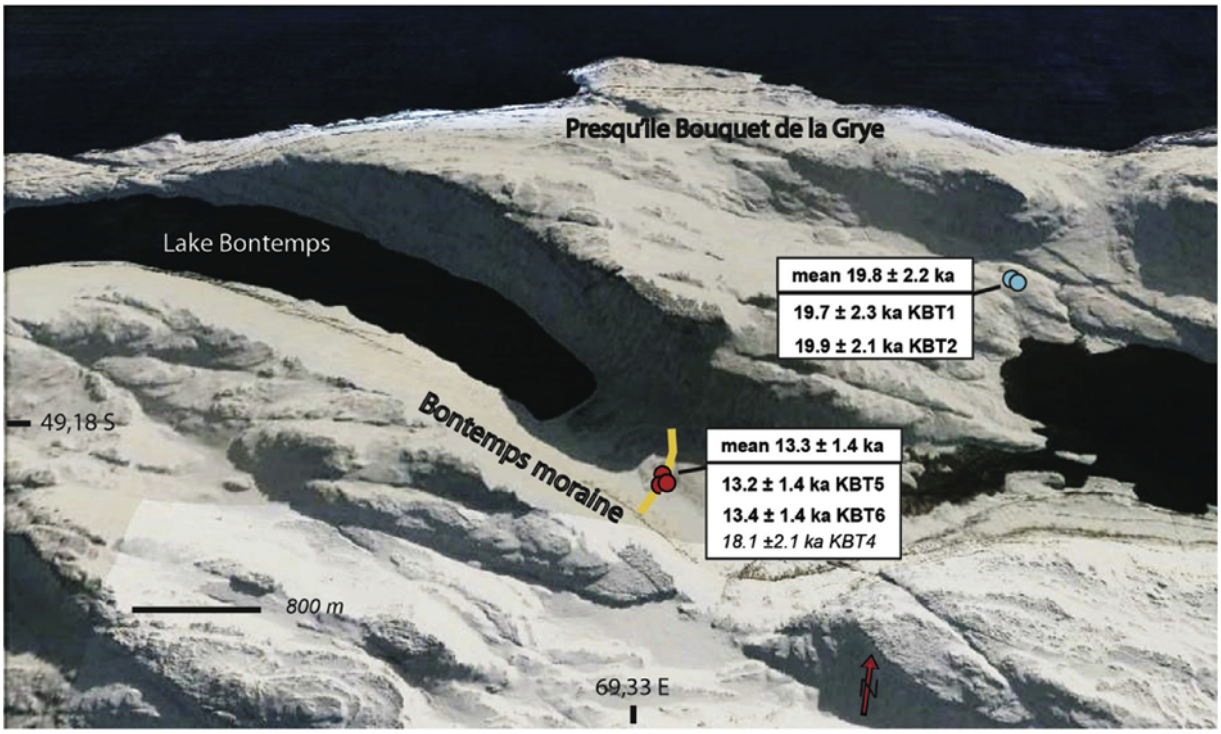

Fig. 3. Sample locations in Bontemps valley and Presqu'ile Bouquet de la Grye with the corresponding individual ^{36}Cl ages. Red circles show samples on Bontemps moraine highlighted by the yellow line, blue circles show erratic boulders on Presqu'ile Bouquet de la Grye. Also shown are the arithmetic means for the age populations with the 1σ uncertainty including standard deviation, analytical and production rate uncertainties. The sample KBT4 in italic was rejected as an outlier based on statistical tests (see text for details). (For interpretation of the references to colour in this figure legend, the reader is referred to the web version of this article.)

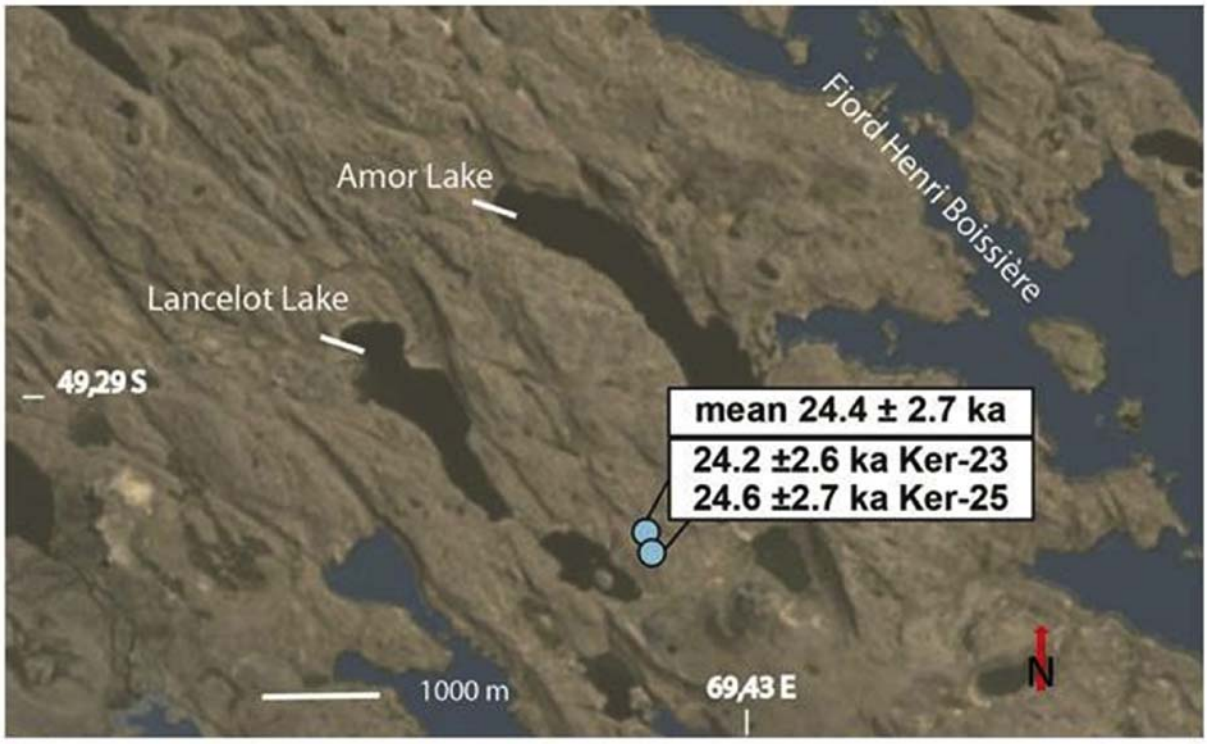

Fig. 4. Location of erratic boulders at Amor lake site with the corresponding individual ^{36}Cl ages and their arithmetic mean. The uncertainties in the individual ^{36}Cl boulder ages account for analytical and production rate uncertainties, while the 1σ uncertainty in the mean includes standard deviation, analytical and production rate uncertainties.

et al., 2015), which is culminating at 1030 m above sea level (a.s.l.). Glaciers are also present on Mont Ross 1850 m a.s.l., the highest summit on Kerguelen. The eastern part of the archipelago forms a peninsula with a mean elevation of 200 m a.s.l., where the scientific station Port-aux-Français (12 m a.s.l.) is located, about 80 km away from the CIC. Here, glaciers are currently absent and the peninsula is characterized by undated glacial and glacio-fluvial deposits and landforms (Hall, 1984), including numerous glacial lakes (Heirman et al., 2012). There is only one permanent weather station located at Port aux Français. Daily values of temperature and precipitation are available since 1951. The climate of Kerguelen archipelago is cool oceanic with a mean annual temperature of 4.6 °C and about 800 mm of precipitation measured at Port aux Français. However, meteorological stations set up in 2010 in the framework of glaciological investigations (IPEV-Kesaaco) on and around the CIC revealed strong spatial precipitation gradients (Verfaillie et al., 2015). The CIC creates a topographic barrier perpendicular to the dominant westerly winds and received a large amount of precipitation, about 3150 mm per year at 250 m a.s.l. between 2010 and 2014 (Favier et al., 2016).

3. Previous work on glacier fluctuations at Kerguelen

Ampere glacier (about 67 km^2 in 2011) is the largest CIC outlet glacier flowing to the south east towards Table Bay, which has been extensively studied over the last decades. Between 1963 and 2006, the retreat of Ampere glacier was 2830 ± 161 m (Berthier et al., 2009) and was associated with the formation of a proglacial lake (Ampere Lake) in 1963 (Fig. 2), which covered an area of 3.5 km^2 in 2010. Using a distributed glaciological model forced by a unique and consistent long-term meteorological and glaciological dataset available since 1951 at Kerguelen, Favier et al. (2016) showed that the CIC experienced a dramatic wastage over the last decades, with ice loss values among the highest in the world. A total loss of 1.6 m water equivalent per year (m w.e. a^{-1}) was measured over the ice cap between 1960 and 2011, and the loss even reached 2.76 m w.e. a^{-1} on Ampere glacier. Favier et al. (2016) demonstrated that precipitation decrease was the first order cause for glacier wastage since the 1960s.

Frenot et al. (1993) identified six moraines between the coast and the present ice margin of Ampere glacier. The authors assigned the timing of formation of these moraines to the last millennium, based on a relative dating technique that uses the radial growth of *Azorella selago* Hook, a cushion-forming Umbelliferae species growing on the moraine. The farthest and most prominent moraine, hereafter named M1, is located about 7 km away from the 2010 front position. Frenot et al. (1993) inferred from the above-mentioned dating method that M1 was formed before the end of the 18th century. The other moraines located at about 300 and 400 m upslope from M1 may have been formed during the 19th and earlier 20th centuries (Frenot et al., 1993).

The recent rapid retreat of Ampere glacier favored the outcropping of organic peat deposits located at about 60 m and 150 m in altitude on the right lateral margin of the glacier, which were radiocarbon dated (Frenot et al., 1997). As these sample sites must have been free of ice at the time corresponding to the formation of the peats with an upstream Ampere glacier front position, the radiocarbon ages were interpreted as reflecting two glacial retreat periods, the first before 13.1–11.2 cal ka BP and the second before 5.0–5.2 cal ka BP (Frenot et al., 1997) (Fig. 2), both ages recalibrated using the Southern Hemisphere SSH13 radiocarbon calibration curve (Hogg et al., 2013).

4. Methods

4.1. Sample sites

Between December 2010 and January 2014, fieldwork was

conducted in the western part of the Kerguelen Islands on the eastern slope of the CIC. Four sites were visited in order to collect rock samples from glacial moraine boulders, erratic boulders (identified as being transported by ice based on their location on flat surfaces, their big size and their shape, Fig. 5) and one roche moutonnée surface: Ampere valley, Bontemps valley, Presqu'ile Bouquet de la Grye and Armor Lake, (sample locations in Fig. 1 and Table 1). These terrestrial investigations were compared with the findings from an offshore bathymetric and coring campaign in 2009 to document possible glacier extensions into the sea in Table Fjord.

In Ampere valley, five samples (Ker-M1-01 to -04, Ker-07; Fig. 2) were collected along the oldest moraine crest M1, and located at an altitude of about 35 m a.s.l. Another sample, Ker-09, was extracted from a roche moutonnée located about 100 m downslope from moraine M1 at 25 m a.s.l.

In Bontemps valley, aerial photo analysis revealed a prominent moraine located about 26 km down-valley from the current ice front. This frontal moraine of about 10 m height and 30 m length with a steep distal slope is covered by sub-angular large boulders (>50 cm in length). It was formed by the CIC outlet Explorateur glacier and dams Bontemps Lake, the largest lake on the main island. On the top of this frontal moraine, samples KBT4, KBT5 and KBT6 were collected at an altitude between 13 and 16 m a.s.l (Fig. 3).

Two other samples KBT1 and KBT2 were collected from erratic boulders, located about 15 m apart from each other at an altitude of 82 m a.s.l. and 69 m a.s.l., respectively, in a small neighbor valley, Presqu'ile Bouquet de la Grye at the base of Mount Von Schleinitz, located 1 km north of Bontemps valley (Fig. 3).

The fourth sample site is located on the south eastern slope of Armor Lake about 38 km away from the CIC (Figs. 4 and 5). Armor Lake is a large fjord-type lake of 3.5 km length, located about 2–4 m a.s.l., above the Fjord Henri Boissière. About 1.5 km south of Armor Lake, two erratic boulders (B023, B025), deposited 100 m apart from each other, were sampled on the basaltic flat plateau at an altitude of 170 m a.s.l.

4.2. *In situ* ^{36}Cl dating

All samples were collected from the uppermost ~3–4 cm of the surfaces of either flat-topped basaltic boulders or roche moutonnée (Table 1), using a hammer and chisel (Fig. 5). We avoided the edges of sampled surfaces, and measured topographic shielding using a clinometer. We recorded geographic coordinates with a handheld GPS device. The elevation was determined from shuttle radar topography mission data (SRTM), which provided better accuracy than the GPS measurements. Whole rock samples were prepared for *in situ* ^{36}Cl dating at CEREGE, Aix-en-Provence, France. First, they were crushed and sieved. An aliquot of bulk rock was sent to the Service d'Analyse des Roches et des Minéraux (SARM, Nancy, France) for major and trace element analysis (Table 2). The bulk rock composition is necessary to compute the low-energy neutron flux in the samples, which controls the ^{36}Cl production from capture of the low-energy neutrons on ^{35}Cl. Due to the mostly low Cl concentrations in the etched samples (see Table 4), this production reaction contributes to between 2% and 22% of the total ^{36}Cl concentrations in the samples.

The grain size fraction 0.25–0.50 mm was etched in a diluted HF/HNO_3 acid mixture to decontaminate from atmospheric ^{36}Cl and from potentially Cl-rich groundmass (Schimmelpfennig et al., 2009). In this step, about 40% of the initial samples were removed. After this pretreatment, 2 g aliquots of the remaining solid sample grains were collected and sent to SARM to analyze the concentrations of the major elements by ICP-OES (Table 3), as Ca, K, Ti and Fe are the target elements for spallogenic/muogenic production of ^{36}Cl. Before total sample dissolution in a suprapur HF/HNO_3 acid mixture, a ^{35}Cl-enriched spike (~99%) was added to each sample for isotope dilution (Ivy-Ochs et al., 2004). The ^{36}Cl extraction then follows the method outlined in Schimmelpfennig et al. (2011). Two chemistry blanks were performed during the procedure (Table 4). ^{36}Cl and Cl concentrations were inferred from the ^{36}Cl/^{35}Cl and ^{35}Cl/^{37}Cl ratios measured by isotope dilution accelerator mass spectrometry at the AMS facility ASTER-CEREGE (Table 4). ^{36}Cl/^{35}Cl ratios were determined by normalizing to a ^{36}Cl standard prepared by K. Nishiizumi (Sharma et al., 1990). The stable ratio ^{35}Cl/^{37}Cl was also normalized to this standard, assuming a natural ratio of 3.127.

Exposure ages were computed with the Excel® ^{36}Cl age calculation spreadsheet published by Schimmelpfennig et al. (2009), taking into account scaling factors (dependent on the geographic locations), sample compositions, corrections for sample thickness, and topographic shielding (Tables 1–4). Scaling factors were calculated with the time-invariant "St" method (Stone, 2000). The following ^{36}Cl production rates, referenced to sea level and high latitude (SLHL), were used: 42.2 ± 4.8 atoms ^{36}Cl (g Ca)$^{-1}$ yr^{-1} for spallation of Ca (Schimmelpfennig et al., 2011), 148.1 ± 7.8 atoms ^{36}Cl (g K)$^{-1}$ yr^{-1} for spallation of K (Schimmelpfennig et al., 2014), 13 ± 3 atoms ^{36}Cl (g Ti)$^{-1}$ yr^{-1} for spallation of Ti (Fink et al., 2000), 1.9 ± 0.2 atoms ^{36}Cl (g Fe)$^{-1}$ yr^{-1} for spallation of Fe (Stone et al., 2005), and 626 neutrons (g air)$^{-1}$ yr^{-1} for the production rate of epithermal neutrons from fast neutrons in the atmosphere at the land/atmosphere interface (Phillips et al., 2001). The value of 160 g cm^{-2} was applied for the high-energy neutron attenuation length. A bulk rock density of 2.4 g cm^{-3} was assumed for all samples. Other parameters for ^{36}Cl production, e.g. that from slow muon capture by Ca and K, remained unchanged in the originally published version of the Excel® spreadsheet (Schimmelpfennig et al., 2009).

All resulting ^{36}Cl ages are shown in Table 4. The ^{36}Cl age uncertainties correspond to 1σ and were determined through full propagation of analytical and production rate errors, unless otherwise stated. When the mean of several individual ages is presented (moraine age or erratic boulders of similar position), we calculated the arithmetic means of the respective boulder age populations, and their uncertainties include the standard deviation and the mean of the individual age uncertainties (including analytical and production rate errors), added by propagation in quadrature. The internal consistency of the samples was tested using both Chi^2 and Chauvenet's criterion tests.

Potential erosion of the sampled surfaces has not been taken into account in the presented ^{36}Cl ages, because surfaces with little signs of erosion were preferred during sample collection and because of the lack of quantitative information on erosion rates since the last deglaciation at Kerguelen. A hypothetical erosion rate of 5 mm kyr^{-1} would increase the oldest ^{36}Cl ages (erratic boulders at Armor Lake) by at most 7% and would have less effect on the younger ages. This is within the uncertainties of the final ^{36}Cl ages and does not affect our conclusions. Similarly, possible snow cover effects were not included in the ^{36}Cl age calculations for several reasons: 1) the present-day annual snow cover duration is very short, ~1.5 months at 90 m altitude and ~3 weeks at 35 m altitude based on glaciological modelling (Verfaillie et al., 2015; Favier et al., 2016); using these snow cover durations would result in an insignificant snow cover correction. 2) As the sampled erratic and morainic boulders are protruding from the surrounding landscape, they are well exposed to the prevailing winds, and the snow cover on their rock surfaces is likely rapidly reduced or even removed. 3) The high internal consistency of each of the boulder age populations at the sites Armor Lake, Bouquet de la Grye, and Bontemps moraine support the hypothesis that both snow cover and erosion

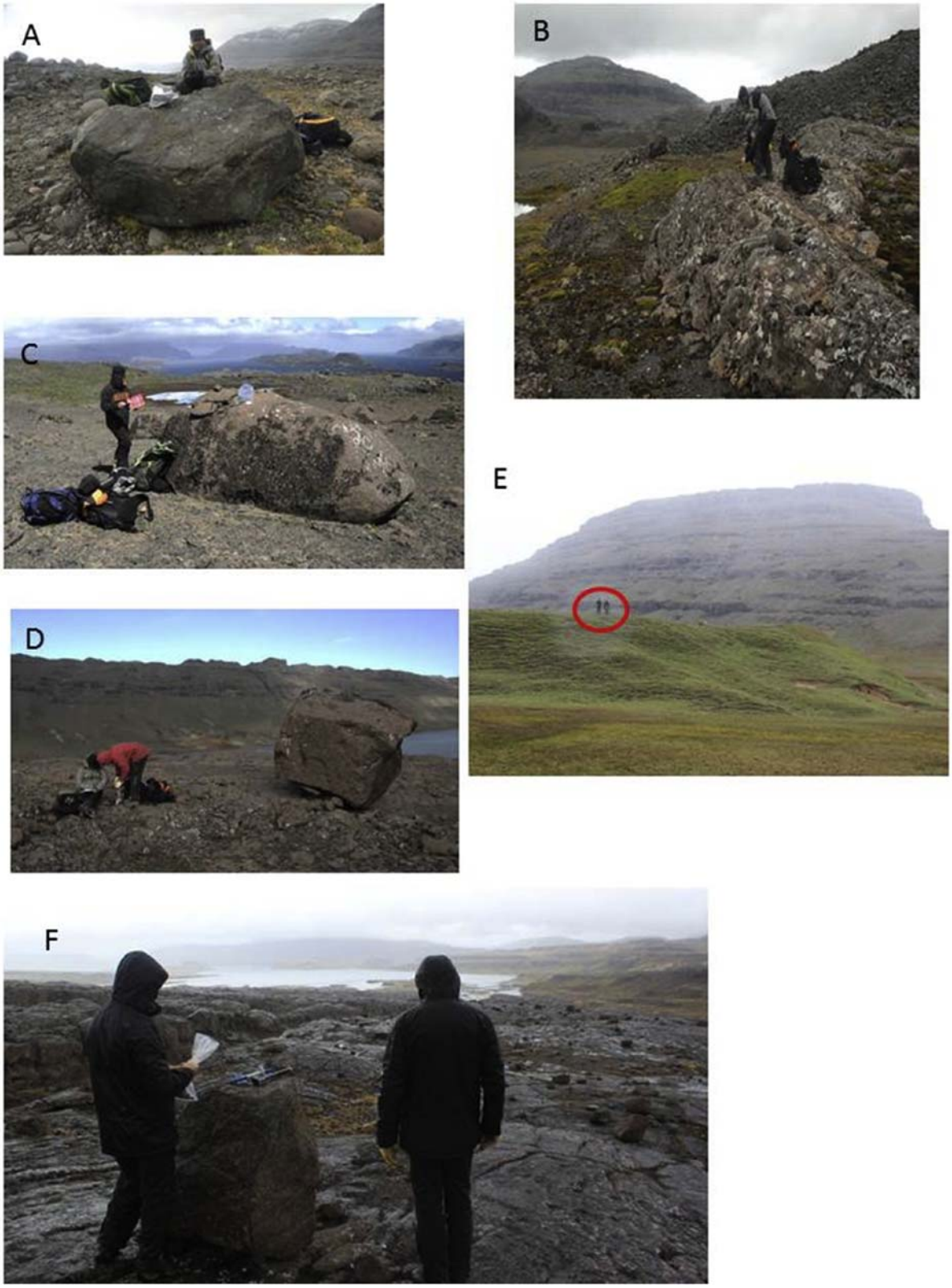

Fig. 5. Pictures of some of the sites sampled during the field campaigns. A: block Ker M1-02 on moraine M1; B: sampling of the roche moutonnée in Ampere valley; C–D: erratic boulders Ker-23 and Ker-25 near Armor lake; E: Bontemps moraine. Note the people in the red circle for scale; F: KBT1 sample on Presqu'ile Bouquet de la Grye. (For interpretation of the references to colour in this figure legend, the reader is referred to the web version of this article.)

Table 2
Chemical compositions of the bulk rock samples before chemical treatment. Analysis performed at the SARM-CRPG (Nancy, France) by ICP-OES (major elements), ICP-MS (trace element), atomic absorption (Li), colorimetry (B) and spectrophotometry (Cl). The bulk of sample Ker-M1-02 was not analyzed, and the composition of Ker-M1-01 was used for the age calculations. See text for details.

Sample Name	Al_2O_3%	CaO %	Fe_2O_3%	K_2O %	MgO %	MnO %	P_2O_5%	TiO_2%	Na_2O %	SiO_2%	CO_2%	LOI %	Total %	Cl (ppm)	Li (ppm)	B (ppm)	Sm (ppm)	Gd (ppm)	Th (ppm)	U (ppm)
Ker-M1-01	12.74	10.74	13.01	0.438	3.54	0.17	0.31	2.74	2.51	47.24	3.38	0.31	100.82	29	3.6	<2	5.97	6.04	1.95	0.39
Ker-M1-03	13.03	10.02	15.32	0.56	5.28	0.21	0.43	3.47	2.85	49.02	0.24	0.43	101.27	100	4.5	<2	7.82	7.69	2.63	0.57
Ker-M1-04	13.85	10.89	11.51	0.27	5.54	0.16	0.24	2.41	2.88	44.96	1.62	0.24	100.64	25	6.6	3	5.05	5.08	1.57	0.32
Ker-M1-07	9.10	4.78	11.13	1.42	2.02	0.10	0.34	2.63	2.20	63.83	0.68	0.34	100.40	<20	23	<2	6.41	6.21	2.56	0.46
Ker-09	10.39	7.43	12.39	0.71	3.79	0.15	0.39	2.83	2.02	57.5	0.48	0.39	100.13	55	15.0	<2	6.80	6.61	2.16	0.46
KBT1	12.88	9.67	15.86	0.49	5.01	0.21	0.47	3.73	2.72	47.02	0.27	0.47	99.96	88	5.3	2	9.49	9.46	2.68	0.50
KBT2	13.60	9.42	14.39	0.78	5.21	0.22	0.36	3.16	2.85	47.06	0.49	0.36	100.51	53	6.5	<2	7.09	6.91	2.15	0.35
KBT4	13.63	8.76	14.797	0.59	4.76	0.20	0.41	3.49	2.92	48.45	0.78	0.41	99.84	93	4.8	<2	7.37	7.14	2.95	0.62
KBT5	13.71	9.38	13.42	0.91	5.19	0.19	0.38	2.96	3.02	49.5	0.23	0.38	99.97	50	4.9	<2	7.43	7.31	2.62	0.55
KBT6	13.79	9.45	13.61	0.80	5.19	0.20	0.38	2.98	3.03	49.27	0.26	0.38	100.42	32	5.2	<2	7.65	7.45	2.60	0.52
Ker- 23	21.11	11.93	8.80	0.70	3.30	0.12	0.22	1.82	2.66	47.52	0.26	1.50	99.68	44	4.6	<2	3.94	3.73	1.69	0.29
Ker- 25	21.03	12.16	8.85	0.66	3.36	0.13	0.22	1.85	2.62	47.69	0.33	1.42	99.99	24	3.6	<2	4.15	4.05	1.70	0.34

Table 3
Concentrations of the ^{36}Cl target elements Ca, K, Ti, and Fe, determined in splits taken from the samples after the chemical pre-treatment (acid etching). Analysis performed at the SARM-CRPG (Nancy, France) by ICP-OES.

Sample Name	CaO %	K_2O %	TiO_2%	Fe_2O_3%
Ampère moraine M1				
Ker-M1-01	8.52 ± 0.17	0.48 ± 0.07	2.97 ± 0.15	9.64 ± 0.19
Ker-M1-02	5.34 ± 0.11	0.14 ± 0.02	3.08 ± 0.15	7.9 ± 0.16
Ker-M1-03	9.78 ± 0.20	0.52 ± 0.03	3.72 ± 0.19	14.96 ± 0.30
Ker-M1-04	2.72 ± 0.14	1.28 ± 0.06	2.54 ± 0.13	11.26 ± 0.23
Ker-M1-07	8.60 ± 0.17	0.25 ± 0.04	2.83 ± 0.14	11.46 ± 0.23
Roche moutonnée				
Ker-09	6.47 ± 0.13	0.57 ± 0.03	2.83 ± 0.14	10.29 ± 0.21
Erratic boulders on Presqu'ile Bouquet de la Grye				
KBT1	9.45 ± 0.19	0.41 ± 0.06	4.36 ± 0.22	15.02 ± 0.30
KBT2	9.01 ± 0.18	0.69 ± 0.03	3.61 ± 0.18	13.35 ± 0.27
Bontemps moraine				
KBT4	8.47 ± 0.17	0.58 ± 0.03	4.19 ± 0.21	14.75 ± 0.20
KBT5	9.32 ± 0.19	0.94 ± 0.05	3.63 ± 0.18	12.64 ± 0.25
KBT6	8.83 ± 0.18	0.82 ± 0.04	3.91 ± 0.20	13.02 ± 0.26
Erratic boulders at Amor lake				
Ker- 23	11.70 ± 0.23	0.56 ± 0.03	1.77 ± 0.09	7.30 ± 0.15
Ker- 25	12.27 ± 0.25	0.51 ± 0.03	1.61 ± 0.08	6.12 ± 0.12

have no significant influence on the ^{36}Cl ages, because otherwise a higher dispersion of the ages would be expected.

4.3. Bathymetry

A survey realized in March 2009 on board R/V Marion Dufresne from the French Polar Institute (IPEV) during the MD172 expedition allowed collecting for the first time multibeam bathymetric data, 3.5 kHz seismic profiles and giant piston cores in the Table Fjord basin. Three cores collected at about 4, 7 and 15 km from the coast, respectively, are presented in this paper to document and date possible marine terminations of Ampere glacier into the Table fjord (Figs. 1 and 6). The core at station A (MD09-3240) is 25 m long and was collected at 169 m water depth offshore the Ampere delta. The core at section 2 (MD09-3239) is 36 m long and was collected at 180 m water depth in the central basin. The core at section C (M09-3238) of 25 m long was collected at 178 m water depth.

As detailed in Table 5 and Fig. 6, six AMS radiocarbon dates were obtained on shell debris (Mollusk shells *Kerguelenis and Signysis*) from Calypso cores MD09-3239 (three samples) and MD09-3238 (three samples) at ARTEMIS, the French national AMS ^{14}C facility. The Table Fjord is ~15 km long and 2 km large and is connected to the Southern Ocean by two sills, the shallower one at 25 m depth and the deeper one around 60 m depth. An estuarine circulation occurs within the fjord with fresh water leaving the fjord at the surface and oceanic water entering at depth. To correct the ^{14}C ages of the core samples for the ^{14}C reservoir age of the fjord, we considered the pre-bomb $\Delta^{14}C$ as estimated from the GLODAP data set (Key et al., 2004). The polar front corresponds to a rapid increase of the $\Delta^{14}C$ to the North (Fig. 7) and its position is currently located either north or south of the Kerguelen archipelago (Roquet et al., 2009). Thus, to calibrate the ^{14}C ages of core samples we used a reservoir age of 900 ± 100 years (corresponding to a $\Delta^{14}C$ of −103 ± 10‰), the Southern Hemisphere SSH13 radiocarbon calibration curve (Hogg et al., 2013) and the oxcal software (Bronk Ramsey and Lee, 2013).

In addition, measurements performed on board R/V Marion Dufresne of sediment magnetic susceptibility, gamma density and P wave velocities on a GEOTEC core scanner with a sampling interval of 2 cm allow characterizing two contrasted sedimentary units associated with different acoustic facies on seismic data (Fig. 8).

Table 4
^{36}Cl dating results, including measured ^{35}Cl/^{37}Cl and ^{36}Cl/^{35}Cl ratios, inferred ^{36}Cl and Cl concentrations, individual sample ages, and mean ages of boulder populations. Procedural blank Bk1 was prepared with all samples but Ker M1-02, Ker 23 and Ker 25, which were prepared with blank Bk2. Spike is enriched in ^{35}Cl (~99.9%). Samples in italic were rejected as outliers and excluded from mean age calculations.

Sample Name	Sample weight (g)	mass of Cl in spike (mg)	^{35}Cl/^{37}Cl	^{36}Cl/^{35}Cl (10^{-14})	[Cl] in sample (ppm)	[^{36}Cl] (10^3 atoms g^{-1})	Age (yr)[a]	Mean age (yr)
Ampère moraine M1								
Ker M1-01	59.416	1.613	13.610 ± 0.061	0.78 ± 0.12	10.4	2.86 ± 0.84	560 ± 210 (200)	
Ker M1-02	62.178	1.598	56.01 ± 0.31	0.85 ± 0.12	1.6	2.27 ± 0.66	890 ± 280 (270)	
Ker M1-03	*63.004*	*1.617*	*5.263 ± 0.016*	*4.49 ± 0.34*	*49.7*	*46.9 ± 3.7*	*7620 ± 990 (780)*	700 ± 320
Ker M1-04	55.147	1.616	8.536 ± 0.042	0.82 ± 0.13	22.2	4.5 ± 1.1	1020 ± 330 (320)	
Ker M1-07	66.554	1.620	26.88 ± 0.20	0.68 ± 0.11	3.9	1.55 ± 0.62	350 ± 170 (160)	
Roche moutonnée								
Ker 09	56.904	1.617	29.16 ± 0.14	10.26 ± 0.48	4.1	54.1 ± 2.7	15700 ± 1700 (1200)	15700 ± 1700
Erratic boulders on Presqu'ile Bouquet de la Grye								
KBT1	43.345	1.618	6.374 ± 0.028	9.49 ± 0.49	47.4	116.7 ± 6.2	19700 ± 2300 (1600)	19800 ± 2200
KBT2	51.976	1.612	41.478 ± 0.28	16.75 ± 0.66	2.9	94.2 ± 3.8	19900 ± 2100 (1400)	
Bontemps moraine								
KBT4	*40.520*	*1.626*	*6.467 ± 0.040*	*7.81 ± 0.46*	*49.5*	*101.2 ± 6.2*	*18100 ± 2100 (1600)*	
KBT5	59.309	1.646	19.61 ± 0.12	12.02 ± 0.52	6.6	66.2 ± 3.0	13200 ± 1400 (980)	13300 ± 1400
KBT6	43.095	1.613	29.16 ± 0.14	9.15 ± 0.44	5.5	63.2 ± 3.2	13400 ± 1400 (1100)	
Erratic boulders at Amor lake								
Ker 23	59.428	1.602	13.446 ± 0.058	25.17 ± 0.73	10.4	149.9 ± 4.4	24200 ± 2600 (1600)	24400 ± 2700
Ker 25	76.064	1.601	15.572 ± 0.030	33.89 ± 0.98	6.7	151.7 ± 4.4	24600 ± 2700 (1600)	
Blanks					**Total atoms Cl (10^{17})**	**Total atoms ^{36}Cl (10^4)**		
Bk1	–	1.623	300.7 ± 5.2	0.395 ± 0.081	2.604 ± 0.067	17.4 ± 2.9	–	–
Bk2	–	1.610	261.5 ± 3.0	0.379 ± 0.085	3.164 ± 0.051	10.6 ± 2.4	–	–

[a] Age uncertainties are reported at 1 sigma level and were calculated through full propagation of analytical and production rate errors. Numbers in brackets are analytical uncertainties only.

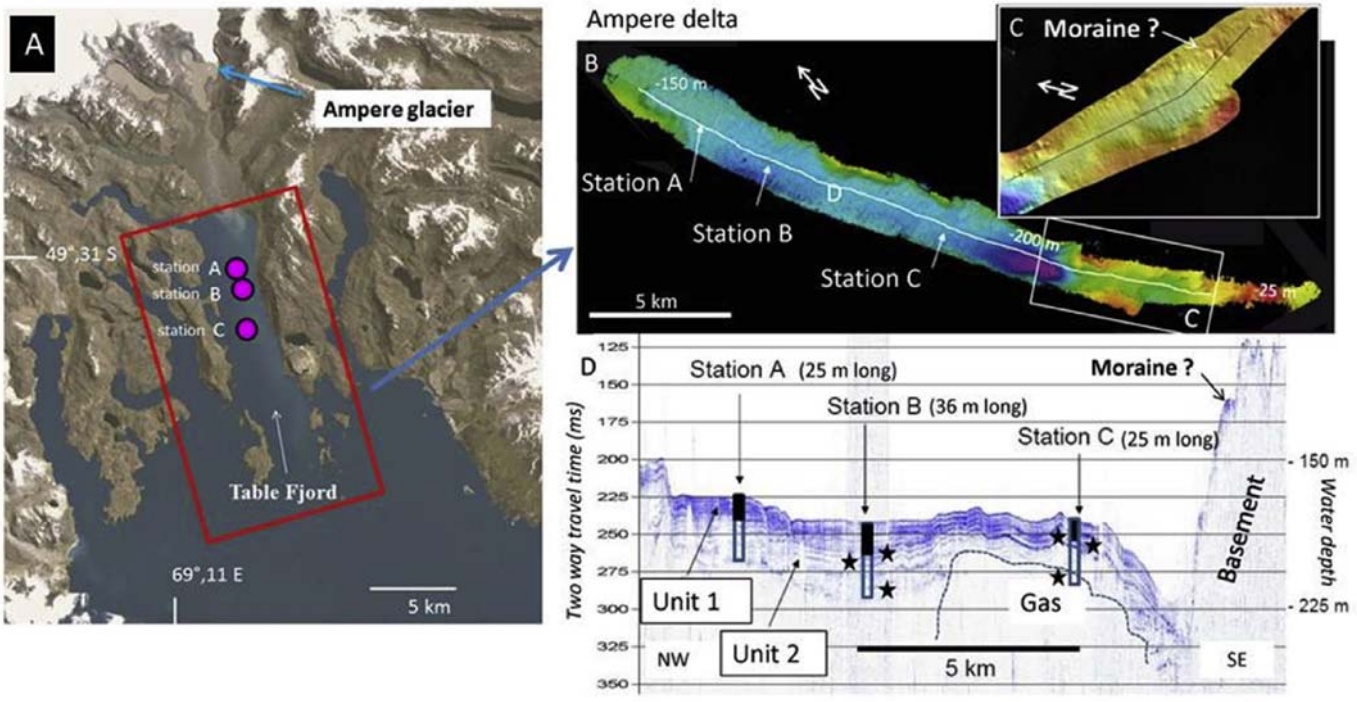

Fig. 6. Ampere glacier and Table Fjord with the three station locations. Table Fjord multibeam bathymetry (B), and a close up section in (C) of the possible feature that may be a moraine deposit in this fjord. White line in B localizes the 3.5 kHz profile along the axis of the fjord detailed in (D) and illustrates the location of giant piston coring stations A, B and C, together with acoustic facies associated with sedimentary units 1 (black rectangle) and 2 (white rectangle) on Calypso cores. Reduced acoustic signal penetration within unit 2 is likely resulting from gas-rich sediments. A peculiar seismic facies on a ridge, identified by both bathymetric data (B, C) and 3.5 kHz data (D), may suggest the development of a glacial deposit (moraine?) formed after the LGM as discussed in the text. Black stars indicate depths of shell debris dated by radiocarbon given in Table 5 and discussed in the text.

Table 5
Radiocarbon ages (calendar ages (CE/BCE) obtained from shell debris sampled in piston cores from Table Fjord at stations B and C shown in Fig. 6. As detailed in the text, these measurements were corrected from a reservoir age and calibrated. Results and uncertainties (2σ probability) allow dating the onset of seismic unit 1 and the base of piston cores collected in the axis of Table Fjord.

Core site	Lab. number	Core depth (m)	Sample type	Age BP	Res. Age	Cor. ^{14}C Age	Age Cal BP	from CE/BCE	to CE/BCE	to CE/BCE	Seismic unit
Station C	SacA 27588	8.19	shell debris	1720 ± 30	900 ± 100	820	720	1135 CE	1310 CE	1276 CE	base Unit 1
Station C	SacA 27591	11.89	shell debris	1930 ± 30	900 ± 100	1030	845	898 CE	1230 CE	1184 CE	upper part Unit 2
Station C	SacA27594	24.35	shell debris	2795 ± 30	900 ± 100	1895	1665	150 CE	396 CE	358 CE	base core, Unit 2
Station B	SacA16125	10.18	shell debris	1580 ± 35	900 ± 100	680	605	1217 CE	1451 CE	1402 CE	basal part Unit 1
Station B	SacA 16126	13.15	shell debris	1785 ± 30	900 ± 100	885	765	1061 CE	1274 CE	1240 CE	top Unit 2
Station B	SacA16139	35.54	shell debris	3975 ± 35	900 ± 100	3075	3180	1400 BCE	1059 BCE	1130 BCE	base core, Unit 2

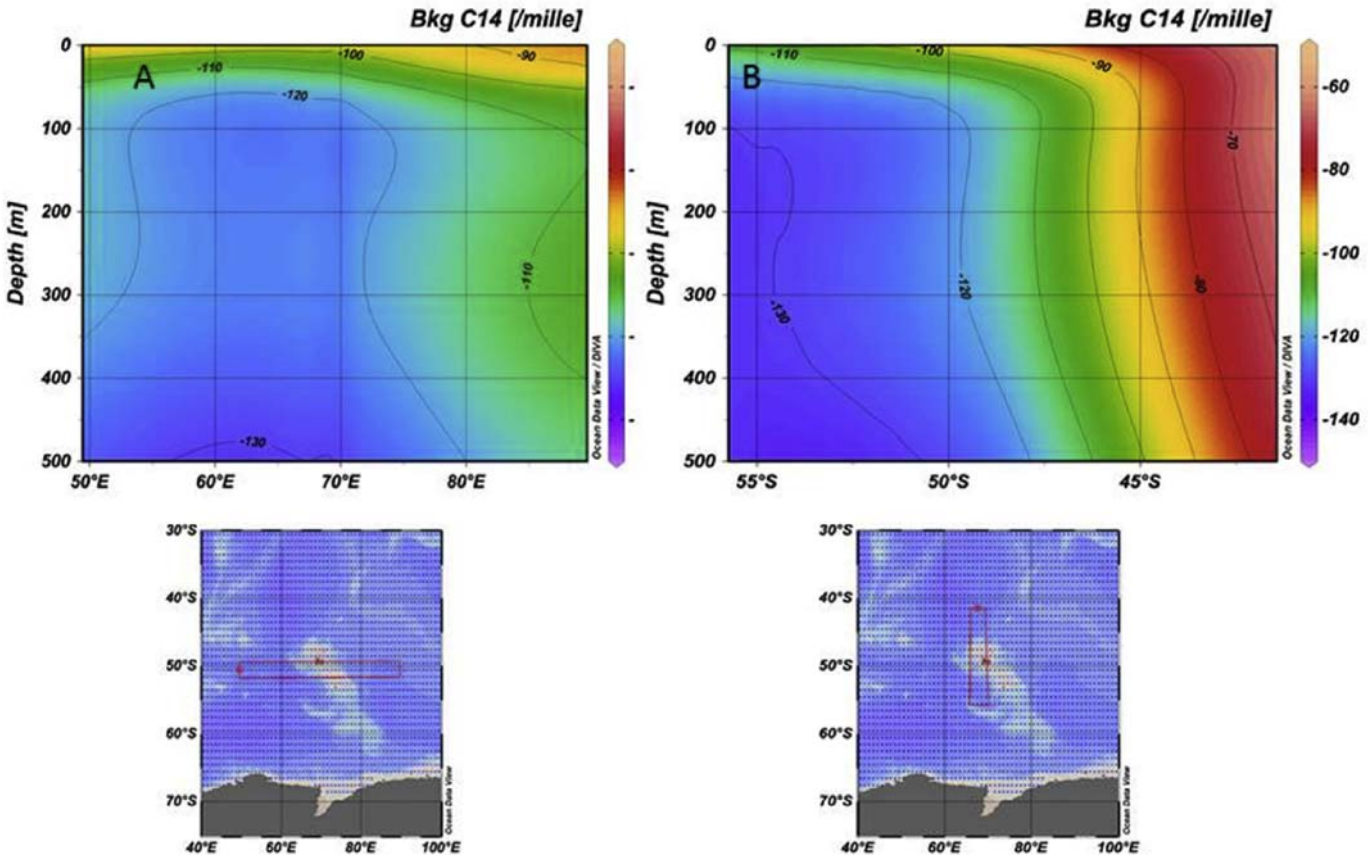

Fig. 7. Longitudinal (A) and latitudinal (B) sections of the natural carbon distribution in the Kerguelen area from GLODAP dataset (Key et al., 2004), plotted with Ocean data View software (Schlitzer, R., Ocean Data View, http://odv.awi.de, 2016).

5. Results

5.1. ^{36}Cl ages from erratics, moraine boulders and roche moutonnée

The ^{36}Cl ages range from ~24.6 to ~0.3 ka (Tables 1–4) and can be divided into two groups in terms of sampled glacial features (Figs. 9 and 10). The first group is composed of the distant erratic boulders at Armor site and Presqu'ile Bouquet de la Grye and the roche moutonnée down valley from moraine M1 in Ampere Valley. The two erratic boulders at Armor site are the oldest in our data set, yielding internally consistent ^{36}Cl ages of 24.2 ± 2.6 ka and 24.6 ± 2.7 ka with a mean age of 24.4 ± 2.7 ka. This sampling site is the farthest in our study, about 38 km from the CIC center, at the highest altitude (170 m a.s.l.). Closer to the CIC (27 km) and at lower altitude (70–80 m a.s.l.), two other erratic boulders collected at Presqu'ile Bouquet de la Grye yield consistent ^{36}Cl ages of 19.7 ± 2.3 ka and 19.9 ± 2.1 ka with a mean age of 19.8 ± 2.2 ka. The roche moutonnée sample is located at about 4.7 km from the current front position of CIC Ampere glacier at an altitude of 25 m a.s.l. and yields a ^{36}Cl age of 15.7 ± 1.7 ka.

The second group is composed of boulders on the top of moraines. In Bontemps valley, three ^{36}Cl ages from the moraine crest are 18.1 ± 2.1 ka, 13.4 ± 1.4 ka and 13.2 ± 1.4 ka. From this dataset, sample KBT4 (18.1 ± 2.1 ka) was rejected as an outlier based on the Chi^2 and Chauvenet's criterion. This moraine boulder likely was pre-exposed to cosmic radiation and reworked during the last glacier advance. The remaining two consistent boulder ages yield a mean of 13.3 ± 1.4 ka (Fig. 10a). A careful aerial photo analysis revealed a clear lack of moraine landforms upstream from Bontemps moraine and in the adjacent valleys, which would have permitted documenting front position changes during later periods, except for some very fresh moraines close to the current front

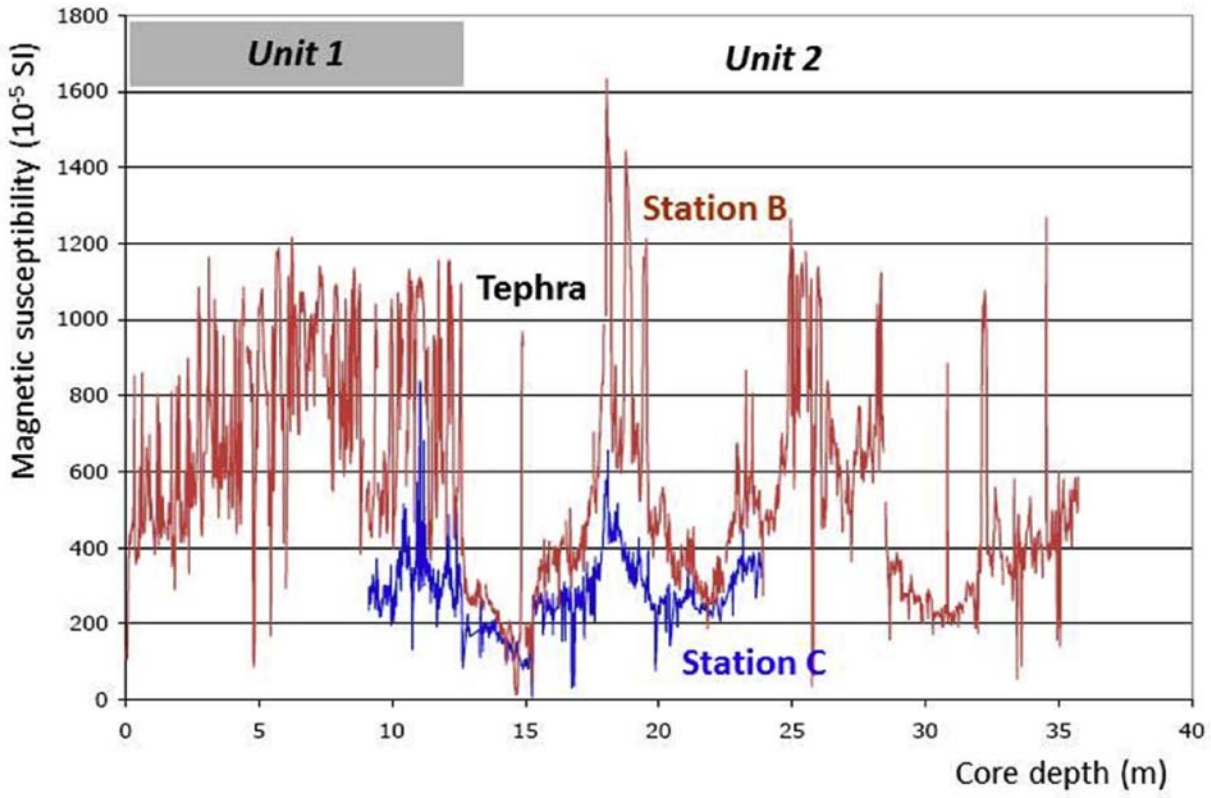

Fig. 8. Correlation of glacio-marine sediment magnetic susceptibility from Calypso cores sampled at stations B and C in Table fjord. In these two cores, the identification of a volcanic layer (tephra) consisting of similar white pumices sands and gravels fully agrees with the evolution of sediment magnetic susceptibility within sedimentary unit 2 at both stations. At station B, sedimentary unit 1 is, however, much thicker and characterized by higher values, suggesting higher sediment supply form the Ampere fluvio-glacial stream in this part of the fjord during recent times as discussed in the text.

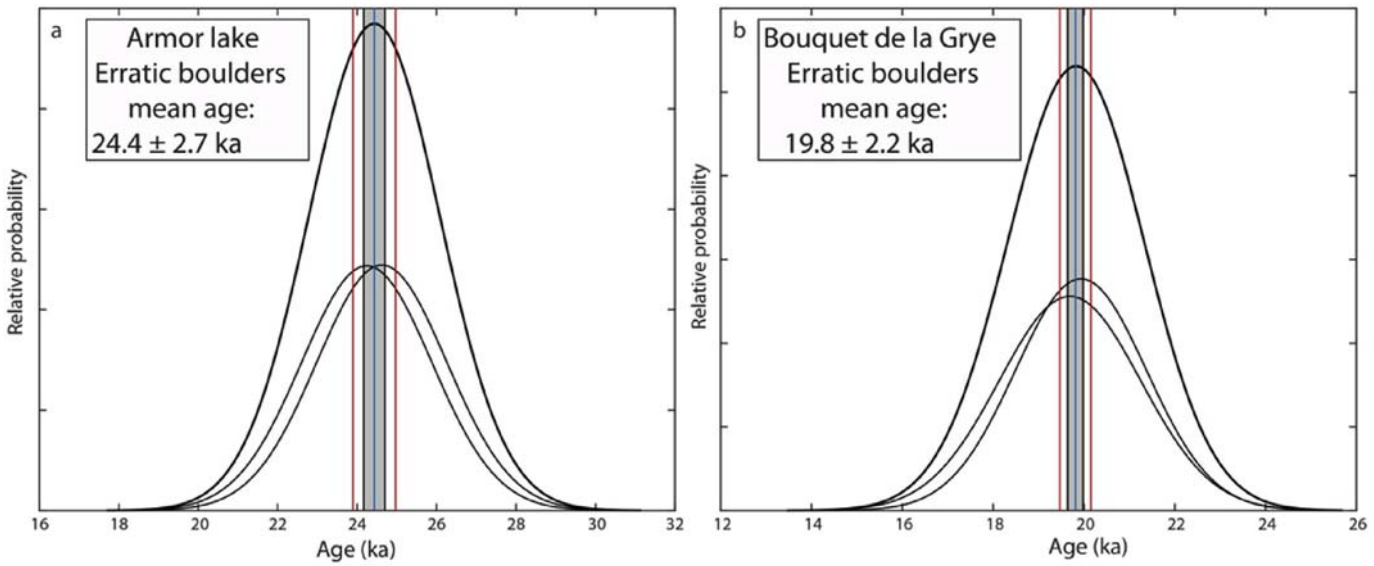

Fig. 9. Probability plots of ^{36}Cl ages from (**a)** Erratic boulders at Armor Lake; (**b)** Erratic boulders at Bouquet de la Grye. The Gaussian curves of the individual ages do not include the ^{36}Cl production rate uncertainties (analytical uncertainties only). Vertical blue line and grey band represent arithmetic mean and standard deviation, respectively. Vertical red lines: 2 σ uncertainty. The error of the mean age in the white box includes the ^{36}Cl production rate uncertainties. (For interpretation of the references to colour in this figure legend, the reader is referred to the web version of this article.)

position, which were formed during the 20th century. In Ampere valley, ^{36}Cl ages of four boulders collected on moraine M1 crest range from 1.02 ± 0.33 ka to 0.35 ± 0.17 ka. In addition, one age (Ker M1-03: 7.62 ± 0.99 ^{36}Cl ka) was rejected as an outlier based on statistical tests, also probably due to pre-exposure. The ^{36}Cl mean age of Ampere moraine M1 is 700 ± 320 a (n = 4), i.e. 1310 ± 320 CE (Fig. 10b).

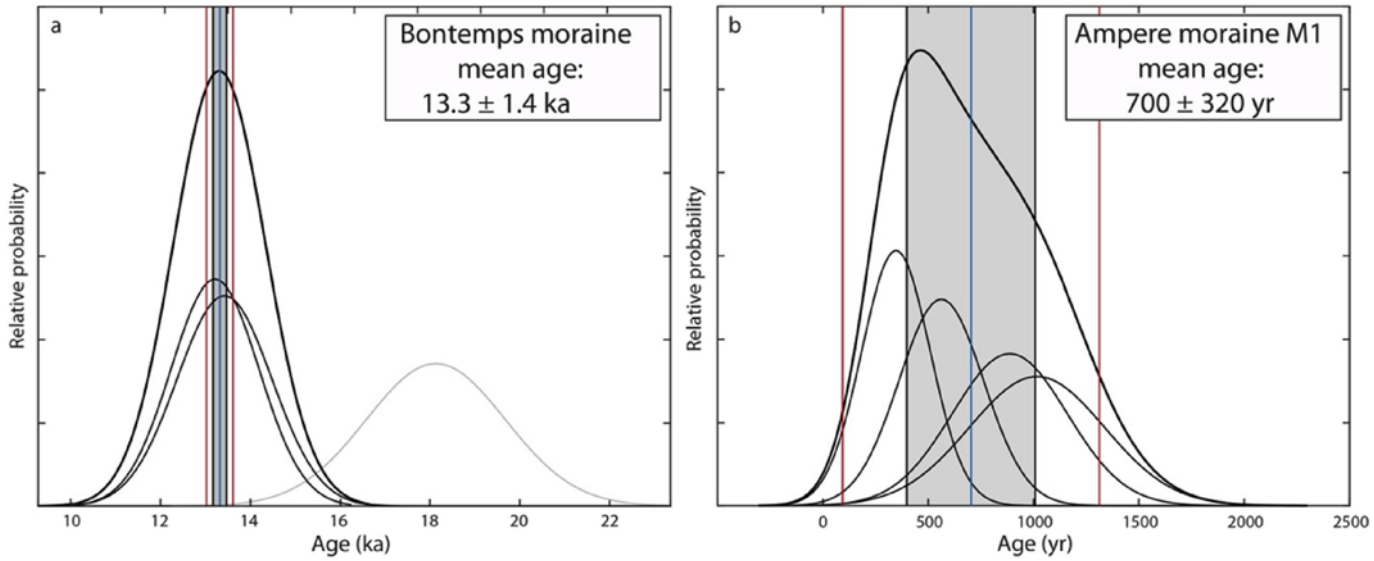

Fig. 10. Probability plots of ^{36}Cl boulder ages from (**a**) Bontemps moraine; (**b**) Ampere moraine M1. The gaussian curves of the individual ages do not include the ^{36}Cl production rate uncertainties (analytical uncertainties only). Grey curve in (a) indicates outlier. Note that the 7.62 ± 0.99 ka outlier has not been included in Fig. 10b. Vertical blue line and grey band represent arithmetic mean and standard deviation, respectively (outliers are not included). Vertical red lines: 2 σ uncertainty. The error of the mean age in the white box includes the ^{36}Cl production rate uncertainties. (For interpretation of the references to colour in this figure legend, the reader is referred to the web version of this article.)

5.2. Table Fjord geomorphology and basin fill

5.2.1. Table Fjord basin fill geometry and nature

Two different seismic units are identified within the upper 40 m of the sedimentary infill of Table Fjord in the basin axis and were sampled by giant piston cores at three sites (Fig. 6). Seismic unit 1 is made of high-frequency and continuous high-amplitude reflections and is thickest at Station B (Fig. 8). This upper seismic unit consists of dark brown bioturbated muds rich in shell debris and characterized by high values in sediment magnetic susceptibility (between 600 and 1200 10^{-5} SI) and gamma-density (between 2 and 2.6 gm/cm^3). Higher values are associated with numerous hyperpycnal flood deposits (these centimetric layers are locally sandy based and erosive at Station A while depositional up to 60 cm thick at Station B). Seismic unit 2 is made of low-frequency continuous high-amplitude reflections and consists of gas-rich brownish bioturbated muds rich in shell debris. On average, these sediments have lower values of magnetic susceptibility (mean around 600 10^{-5} SI) and gamma density (mean around 1.8 gm/cm^3) than unit 1. However, several horizons with higher values similar to those of seismic unit 1 are identified either at stations A, B or C and correlated with continuous and higher amplitude reflections identified on seismic data.

The base of the sedimentary infill of Table Fjord is not visible on 3.5 kHz data and the acoustic signal is absorbed by gas rich sediments in the lower part of seismic unit 2 at the bases of giant piston cores.

5.2.2. Table Fjord basin fill chronology

Six AMS radiocarbon ages of shell debris collected close to the transition between seismic unit 1 and seismic unit 2 and at the base of the cores from station B and C do not exceed the last 4 ka cal BP (Table 5) and thus suggest very high sedimentation rates during the Late Holocene in the fjord. The onset of unit 1 is dated to 1110–1290 CE (2 σ) and suggests an increase in the mean sedimentation rate during the last millennium when applying a deposition model and using the oxcal software (Bronk Ramsey and Lee, 2013).

6. Discussion

6.1. Interpretation of Table Fjord sedimentary record

Offshore from the Ampere delta and between 150 and 225 m water depths, the fjord basin axis is filled with sediments and surrounded by steep lateral slopes made of basaltic rocks, which regionally outcrop above sea level and develop large cliffs along the flanks of the fjord.

The combination of multibeam bathymetry and seismic data highlight no obvious glacial deposits at the sea bed or within the upper ~40 m of the fjord sedimentary infill (Fig. 6). However, we interpret units 1 and 2 as typical well-stratified glacio-marine deposits identified offshore from the Ampere delta draining the Ampere glacier and Ampere valley (Syvitski, 1991; Van Rensbergen et al., 1999; St-Onge et al., 2012). Glacio-marine sedimentation is known to be strongly influenced by clastic sediment supply resulting from glacier fluctuations in the catchment area (Syvitski, 1991; Mulder and Chapron, 2011; Heirman et al., 2011). Higher acoustic amplitudes within seismic unit 1 can be related to enhanced clastic sediment supply identified in piston cores at stations A, B and C both from higher values in sediment magnetic susceptibility (Fig. 8) and gamma density (not shown). Available radiocarbon data from piston cores at station B and C allow dating the onset of this major change in sedimentation pattern in the fjord between 1110 and 1290 CE (2 σ). This change is contemporaneous (within errors) to the development of moraine M1 in the Ampere valley dated at 1310 ± 320 CE and suggests that enhanced clastic sediment supply in Table Fjord reflects increased glacial activity of the CIC during the last millennium.

The distal south-eastern part of the fjord is free of recent sediments and the acoustic basement identified on 3.5 kHz data outcrops between ~225 and 25 m water depths and develops the main sill of this former glacial valley. As shown in Fig. 6B–C, at 23 km from the Ampere glacier front and on the distal slopes of Table Fjord, a 1 km long and 4 m high ridge is observed on the bathymetric data. This landform may correspond to a glacial deposit (e.g. a frontal moraine) and may thus represent the only

geomorphological evidence constraining the evolution of the Ampere Glacier during the last glacial stage. The seismic facies of this ridge indeed contrasts with the surrounding facies of the basaltic basement (Fig. 6C–D) and is similar to the one frequently observed on 3.5 kHz data at the base of glacial lakes or fjord sedimentary basins at mid latitudes (Syvitski, 1991; Vasskog et al., 2011; Heirman et al., 2011, 2012; Viel et al., 2015). An alternative hypothesis is that the topographic sill of Table fjord at 25 m water depth observed only on bathymetric data (Fig. 6B) may partially result from a glacial maximum terminal moraine complex, as recently documented in some fjords of South Georgia (Hodgson et al., 2014b). Both interpretations need to be confirmed by the analysis of box coring samples taken on these ridges in Table Fjord.

6.2. History of CIC glacier fluctuations

^{36}Cl CRE dating of glacial erratics and morainic boulders collected at different sites of Kerguelen Archipelago combined with ^{14}C ages from sedimentary deposits on the Table Fjord provide the first temporal constraints of the retreat history of the CIC since the LGM. The earliest evidence of CIC retreat comes from erratic boulders located close to Armor Lake indicating that retreat likely began 24.4 ± 2.7 ka ago (Fig. 11). The exact extent of the CIC during the global LGM is unknown, but it probably exceeded the current front position by ~20 km, as revealed by the location of the two other erratics deposited ~20 ka ago (samples KBT1 and KBT2 in Fig. 3). During the Late Glacial, the Explorateur glacier experienced a major advance or stillstand at about ~13 ka ago, which formed the moraine in Bontemps valley (26 km from the current front position) most likely during the ACR chronozone (14.5–12.9 ka). However, due to the uncertainties in our ^{36}Cl ages, we cannot exclude that this moraine formation occurred during the Younger Dryas (YD, 12.9–11.6 ka) or during an older period. The marine landform interpreted as a moraine in Table Fjord located ~23 km away from Ampere outlet glacier may correspond to the same episode according to their similar distance from the CIC. However, a higher resolved bathymetric survey combined with ^{14}C ages from this sedimentary deposit are needed before any robust conclusion about possible synchronous glacier advances in Ampere and Bontemps valleys. So far, we could not find any geomorphic evidence of Holocene glacier fluctuations pre-dating the last millennia, supporting the suggestion by Frenot et al. (1997) that Ampere glacier was smaller than today during the early and middle Holocene, based on the ^{14}C ages in the peat formation upstream of Ampere Lake (Fig. 2). Located at a higher altitude than the current front position of Ampere glacier, these peat deposits were formed after the glacier retreated in the early and mid-Holocene periods. A readvance occurred during the late Holocene period covering the peat sample location and formed moraine M1 (Frenot et al., 1997). Finally, the most recent retreat period started in the last centuries (Frenot et al., 1993; Favier et al., 2016). The interpretation of sediment cores in Table Fjord (Figs. 6 and 8) corroborates a shrinking period during the early Holocene, and fluctuations in glacio-marine sediment magnetic susceptibility (Fig. 8) suggest that the glacier

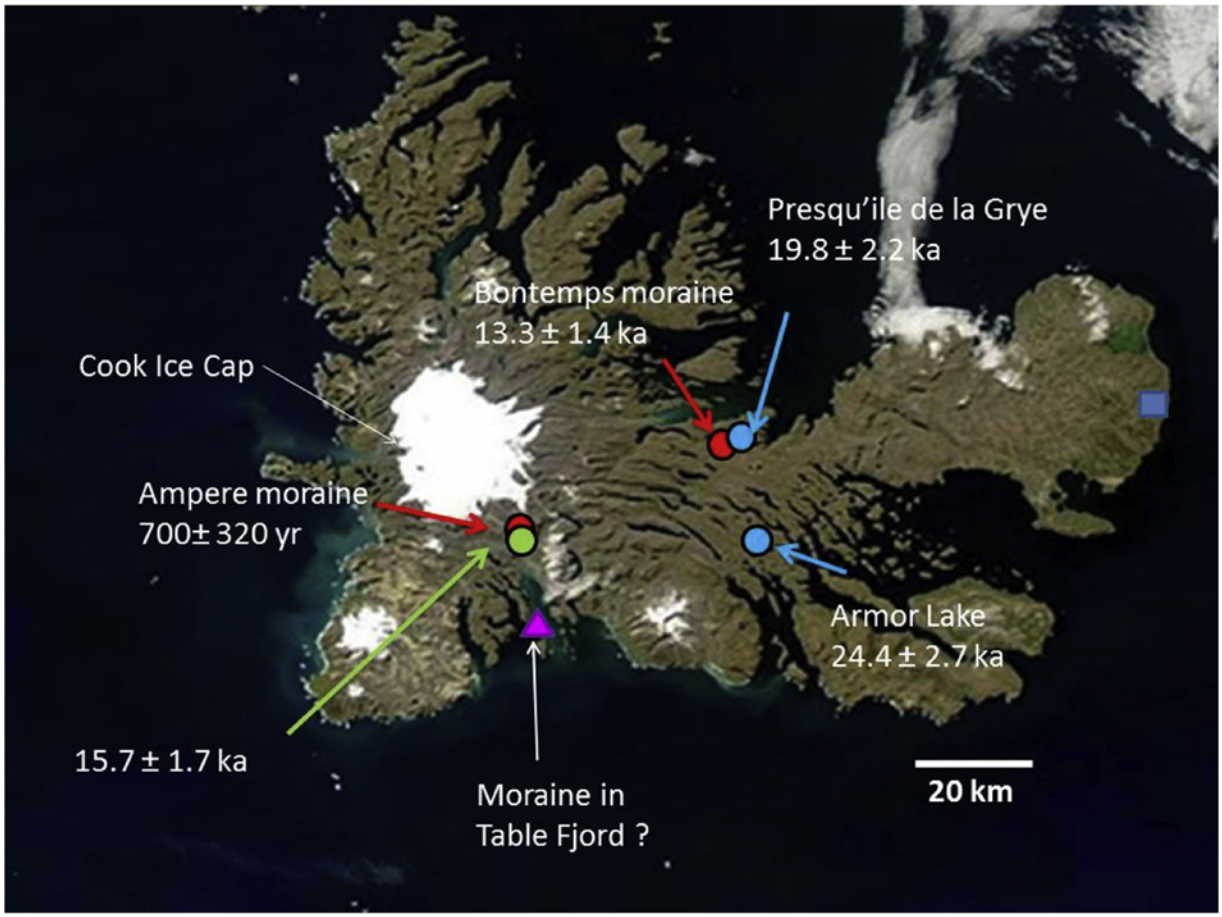

Fig. 11. Summary of ^{36}Cl ages obtained at different sample sites. Reported mean ^{36}Cl boulder ages account for analytical and production rate uncertainties. Red dots = moraine ages; Blue dots = erratic ages; Green dot = age of a roche moutonnée; Purple triangle = landform interpreted as a moraine from bathymetric survey; Blue square = peat sample from Van der Putten et al. (2015). (For interpretation of the references to colour in this figure legend, the reader is referred to the web version of this article.)

started to grow again in the late Holocene but did not reach the sea at least over the last 3000 years. Therefore, evidence of the latest glacier advance/stillstand period is indicated by a series of frontal moraines in Ampere valley, located at ~5 km from the seashore, with the outmost ridge (M1) dated to 1310 ± 320 CE (Fig. 11). This moraine M1 attests to the maximum glacial extent of Ampere glacier during the last millennium and possibly (within errors) during the so-called Little Ice Age (~1450–1850 CE) in agreement with previous studies (Frenot et al., 1993). Bathymetric survey combined with the ^{36}Cl age of the roche moutonnée (sample Ker 09), located slightly down-valley from moraine M1, suggest that Ampere glacier had retreated to this area by ~16 ka ago, thus implying that the last millennium M1 moraine may correspond to the maximum Holocene glacier extent. However, more data are needed to support this hypothesis, because we cannot exclude that the roche moutonnée surface has been pre-exposed during earlier periods of deglaciation, resulting in inherited ^{36}Cl concentrations in this sample.

6.3. Comparison with other paleo glacier records in southern mid latitudes regions

Moraine records in Patagonia and New Zealand show several episodes of ice advance during the LGM and late glacial periods. In both regions, glacial culminations were recorded between 25 ka and 18 ka (e.g. Hein et al., 2010; Kaplan et al., 2011; Putnam et al., 2013a). Although potential (a)synchronies between glacier patterns at Kerguelen and the other sub Antarctic regions should be handled with care due to the large uncertainties of our ^{36}Cl ages, erratic boulders dated to 24 ka suggest that glaciers at Kerguelen were retreating at that time and may have experienced an earlier culmination than in the two other regions. Moreover, unlike in Patagonia and New Zealand, evidence of glacier advances between 19 and 15 ka is so far missing at Kerguelen. Conversely, a possible ACR advance occurred at Kerguelen synchronous with advances in other southern mid (e.g. Fogwill and Kubik, 2005; Putnam et al., 2010; Kaplan et al., 2010, 2011; Moreno et al., 2015; Darwill et al., 2016) and even low latitude regions (Jomelli et al., 2014).

During the Holocene, several glacier advances were identified in the early and late Holocene period in Patagonia and New Zealand (Douglass et al., 2006; Putnam et al., 2010). The detailed moraine record of Mueller glacier in New Zealand (Schaefer et al., 2009) shows at least eleven advances during the late Holocene with a progressive long term decreasing extent. During the Holocene, glaciers at Kerguelen likely experienced a very different glacier behavior compared to the other southern mid latitude regions, with a glacier advance period during the late Holocene that culminated during the last millennium.

6.4. Climate forcing for CIC retreat

The chronological data presented here raise questions about the climate mechanisms underlying the CIC retreat patterns. Our glacier record at Kerguelen depicts a remarkable synchronous behavior with temperature and precipitation changes recently documented by δ^{18}O variations and snow accumulation rate changes in the West Antarctica ice core (WAIS divide Project Members, 2013; Fig. 12). Such common pattern may be due to the fact that the locations of these two studies are affected by marine climate conditions, in contrast to East Antarctica ice cores that are more under the influence of continental climate conditions.

The West Antarctica ice core shows that the most depleted δ^{18}O values at ~26 ka precede a rapidly increasing trend until the Holocene, only interrupted during the cold ACR episode. During the Holocene, the recorded progressive δ^{18}O increase until the late Holocene is followed by more depleted values during the last millennium, in agreement with observations from other West Antarctica areas (Goosse et al., 2012). These δ^{18}O variations reflect atmospheric temperature conditions resulting from ocean circulation and sea ice changes driven by local insolation increase (WAIS divide Project Members, 2013).

The onset of significant warming at 26 ka is in concordance with the timing of erratic boulder deposition at Armor lake. The rapid warming during the Late glacial interrupted during the ACR also agrees remarkably well with the strong glacier retreat at Kerguelen documented by erratic boulders at Presqu'ile Bouquet de la Grye and the re-advance of Explorateur glacier that led to the Bontemps moraine deposition. Finally, the progressive cooler temperature trend from the late Holocene to the last millennium is in agreement with both Table Fjord sediment cores and the Ampere moraine record.

Moreover, the resolution between 23 and 14 ka of the WAIS ice-core record made it possible to document the snow accumulation rate at a centennial time scale (not shown), which resembles the δ^{18}O changes. The accumulation of snow, low and stable between 23 and 19 ka, strongly increased until 14.5 ka, followed by a decrease between 14.5 and 14.0 ka, the end of the measurements. This increase during the late glacial period (19–14.5 ka) is interpreted as resulting from more frequent or stronger moisture-bearing storms penetrating into West Antarctica, which supports a southward shift or intensification of the mid-latitude storm track (WAIS divide Project Members, 2013). The latitudinal position of the storm track is mainly driven by the Southern Annular Mode (SAM) whose positive phase (SAM+) is associated with a belt of low pressure surrounding Antarctica (Thompson and Wallace, 2000; Thompson et al., 2011). The SAM+ (southern position of the storm track) is coupled with increased poleward flow and warm conditions reflected in the WAIS δ^{18}O record and in reduced sea ice in the region (e.g., Lefebre et al., 2004; Marshall, 2007; WAIS divide Project Members, 2013). Under the current climate conditions, a SAM+ is conversely associated with dry conditions in the Kerguelen Islands (Favier et al., 2016).

Such a southward shift of the mid-latitude storm track between 19.0 ka and 14.5 ka is in agreement with a continuous organic sequence recorded at Courbet Peninsula, on the eastern part of the main Kerguelen Island (Fig. 11) (Van der Putten et al., 2015), whose age spanning from 15.8 cal ka BP to 10.9 cal ka BP partly overlaps the period of accumulation measurements. The multi-proxy analysis approach (pollen and plant macrofossils, magnetic susceptibility, XRF analyses, biogenic silica content and humidification degree) suggests a progressive change towards warmer and drier conditions interrupted during the ACR period, which is characterized by very humid and windy conditions.

Consequently, temperature changes depicted at the West Antarctic drilling site agree with CIC advances during the LGM, the ACR and the last millennium. Glacier retreat at CIC between 19.0 ka and 14.5 ka may have also been caused by a decrease in precipitation due to a SAM+ (southward position of the mid latitude storm track) that reversed the snow accumulation pattern at WAIS divide (increase in accumulation). This hypothesized influence of the SAM on glaciers at Kerguelen in the past is supported by recent observations revealing that the unprecedented SAM+ situation over the last millennium (Abram et al., 2013) was the main driver of recent dryness at Kerguelen and of the resulting dramatic wastage of CIC over the last five decades (Favier et al., 2016).

7. Conclusion

This paper presents the first direct glacier chronology in the Kerguelen Islands based on 13 cosmogenic ^{36}Cl surface exposure

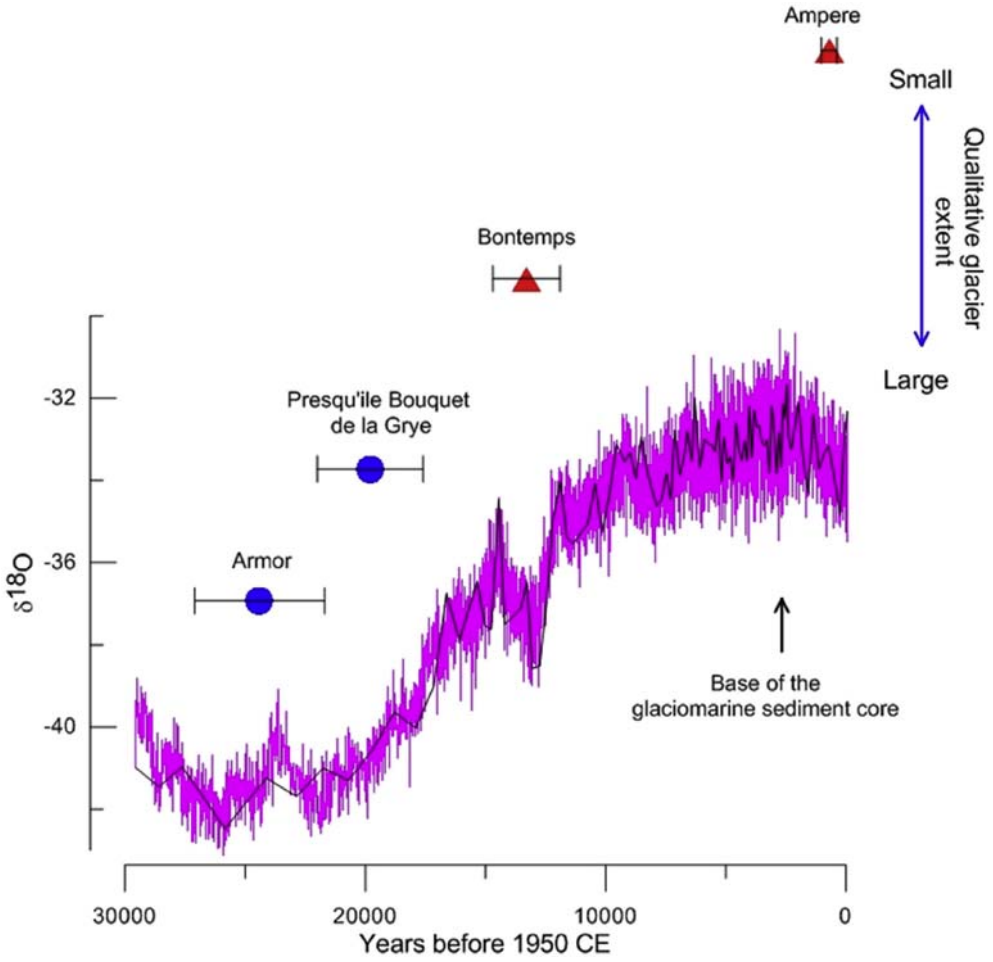

Fig. 12. West Antarctic $\delta^{18}O$ and Kerguelen glacier records. Purple: water isotope ratio from WAIS (West Antarctic Ice sheet Divide Ice core, 2013). Black curve: Spline smoothing. Blue circle: mean erratic boulder age at Armor site and Presqu'ile Bouquet de la Grye. Red triangle: mean moraine age at Bontemps and Ampere sites. The errors of the mean ages include the ^{36}Cl production rate uncertainties. (For interpretation of the references to colour in this figure legend, the reader is referred to the web version of this article.)

ages from boulders on moraines formed by the Explorateur and Ampere glaciers and from erratics and a roche moutonnée surface. Combined with a multibeam bathymetric data and radiocarbon ages from glacio-marine sediment cores collected in Table Bay draining the Ampere glacier, we document the glacier evolution in this sub-Antarctic region. CIC outlet glaciers retreated during the Late Glacial and possibly as early as ~24 ka with an interruption during the time of the ACR period. Glaciers continued to retreat during the Holocene probably until the last 3 ka ago. The last glacial advance (moraine M1 of Ampere glacier) of the CIC is dated to 700 ± 320 yr ago and is reflected by the onset of a major change in Table Bay glacio-marine sedimentation consisting of a strong increase of clastic sediment supply during the Little Ice Age period. The remarkable concomitance between temperature and snow accumulation changes documented from the West Antarctica ice core and glacier changes at Kerguelen suggest strong large scale climate drivers possibly related to the SAM. As Kerguelen is the largest currently heavily glaciated archipelago in the sub-Antarctic region, these findings offer the valuable opportunity to better understand climate change in southern polar regions.

Author contributions

V.J., D.B., D.V., V.R., C.L. and V.F. conducted the field work on the Island; I.S. and F.M. participated in producing the cosmogenic data, ASTER Team performed AMS measurements; I.S., V.M., V.R. and V.J. interpreted the cosmogenic ages; E.M., E.C. and A.J. conducted the field work on Table Fjord, participated in producing the bathymetric data and its interpretation, D.B., V.J. and I.S. prepared figures and V.J., I.S., E.C., V.R., V.F., D.V. and D.S. contributed to writing the paper.

Acknowledgments

This paper was supported by the French INSU LEFE Glacepreker project and by the IPEV Kesaaco 1048 project. We thank the IPEV crew and captain of the MD172 KAVIAR/TABLE expedition for the collection of oceanographic, acoustic and giant piston core data within Table Fjord despite challenging climatic conditions. We thank the team from TRACK program for their great help on handling cores on board. This study benefited from the support of ARTEMIS radiocarbon French facilities from CNRS INSU. Patrick Albéric (ISTO, France), Fabien Dewilde and Nicolas Caillon are also warmly thanked for their contribution to the success of MD172 KAVIAR/TABLE expedition and support for the Geotek data acquisition on board and in the collection and interpretation of radiocarbon data from Table Fjord sediments. The Cl-36 and Cl measurements were performed at the ASTER AMS national facility (CEREGE, Aix-en-Provence) which is supported by the INSU/CNRS, the ANR through the “Projets thématiques d'excellence” program for the “Equipements d'excellence” ASTER-CEREGE action, and IRD.

We thank C. Darwill and an anonymous reviewer for their very constructive remarks.

References

Aniya, M., 2013. Holocene glaciations of Hielo Patagonico (Patagonia Icefield), South America: a brief review. Geochem. J. 47, 97–105.

Bentley, M.J., Evans, D.J.A., Fogwill, C.J., Hansom, J.D., Sugden, D.E., Kubik, P.W., 2007. Glacial geomorphology and chronology of deglaciation, South Georgia, sub-Antarctic. Quat. Sci. Rev. 26, 644–677.

Berthier, E., Le Bris, R., Mabileau, L., Testut, L., Rémy, F., 2009. Ice wastage on the Kerguelen Islands (49°S, 69°E) between 1963 and 2006. J. Geophys. Res. 114, F03005.

Bronk Ramsey, C., Lee, S., 2013. Recent and planned developments of the program OxCal. Radiocarbon 55, 720–730.

Darwill, C.M., Stokes, C.R., Bentley, M.J., Evans, D.J.A., Lovell, H., 2016. Dynamics of former ice lobes of the southernmost Patagonian Ice Sheet based on a glacial landsystems approach. JQS. http://dx.doi.org/10.1002/jqs.2890.

Douglass, D.C., Singer, B.S., Kaplan, M.R., Mickelson, D.M., Caffee, M.W., 2006. Cosmogenic nuclide surface exposure dating of boulders on last-–glacial and late-–glacial moraines, Lago Buenos Aires, Argentina: Interpretive strategies and paleoclimate implications. Quat. Geochronol. 1, 43–58. http://dx.doi.org/10.1016/j.quageo.2006.06.001.

Favier, V., Verfaillie, D., Berthier, E., Menegoz, M., Jomelli, V., Kay, J.E., Ducret, L., Malbéteau, Y., Brunstein, D., Gallée, H., Young-Hyang Park, Y., Rinterknecht, R., 2016. Atmospheric drying as the main driver of dramatic glacier wastage in the southern Indian Ocean. Sci. Rep. 6, 32396. http://dx.doi.org/10.1038/srep32396.

Fink, D., Vogt, S., Hotchkis, M., 2000. Cross-sections for ^{36}Cl from Ti at $E_p = 35–150$ MeV: applications to in-situ exposure dating. Nucl. Instrum. Meth. Phys. Res. Sect. B 172, 861–866.

Fogwill, C.J., Kubik, P.W., 2005. A glacial stage spanning the Antarctic cold reversal in torres del Paine (51°S), Chile, based on preliminary cosmogenic exposure ages. Geogr. Ann. Ser. A Phys. Geogr. 87, 403–408.

Frenot, Y., Gloaguen, J.C., Picot, G., Bougère, J., Benjamin, D., 1993. Azorella selago Hook. used to estimate glacier fluctuations and climatic history in the Kerguelen Islands over the last two centuries. Oecologia 95, 140–144.

Frenot, Y., Gloaguen, J.C., Van De Vijver, B., Beyens, L., 1997. Datation de quelques sédiments tourbeux holocènes et oscillations glaciaires aux Iles Kerguelen. Comptes Rendus l'Académie Sci. 320, 567–573.

Goosse, H., Braida, M., Crosta, X., Mairesse, A., Masson-Delmotte, A., Mathiot, P., Neukom, R., Oerter, H., Philippon, G., Renssen, H., Stenni, B., van Ommen, T., Verleyen, E., 2012. Antarctic temperature changes during the last millennium: evaluation of simulations and reconstructions. Quat. Sci. Rev. 55, 75–90.

Hall, K., 1984. Evidence in favour of an extensive ice cover on sub Antarctic Kerguelen Island during the last glacial. Pal Pal Pal 47, 225–232.

Hein, A.S., Hulton, N.R.J., Dunai, T.J., Sugden, D.E., Kaplan, M.R., Xu, S., 2010. The chronology of the Last Glacial Maximum and deglacial events in central Argentine Patagonia. Quat. Sci. Rev. 29, 1212–1227.

Heirman, K., de Batist, M., Charlet, F., Moernaut, J., Chapron, E., Brummer, R., Pino, M., Urrutia, R., 2011. Detailed seismic stratigraphy of Lago Puyehue: implications for the mode and timing of glacier retreat in the Chilean Lake District. J. Quat. Sci. 26, 665–674.

Heirman, K., de Batist, M., Arnaud, F., de Beaulieu, J.L., 2012. Seismic stratigraphy of the late Quaternary sedimentary infill of Lac d'Armor (Kerguelen archipelago): a record of glacier retreat, sedimentary mass wasting and southern Westerly intensification. Antarct. Sci. 1–11. http://dx.doi.org/10.1017/S0954102012000466.

Hodgson, D.A., Graham, A.C.G., Roberts, S.J., Bentley, M.J., ÓCofaigh, C., Verleyen, E., Jomelli, V., Favier, V., Brunstein, D., Verfaillie, D., Colhoun, E.A., Saunders, K., Mackintosh, A., Hall, K., McGlone, M.S., Van der Putten, N., 2014a. Terrestrial and marine evidence for the extent and timing of glaciation on the sub-Antarctic islands. Quat. Sci. Rev. 100, 137–158. http://dx.doi.org/10.1016/j.quascirev.2013.12.001.

Hodgson, D.A., Graham, A.C.G., Griffiths, H.J., Roberts, S.J., Cofaigh, C.O., Benthley, M.J., Evans, D.J.A., 2014b. Glacial history of sub-Antarctic South Georgia based on the submarine geomorphology of its fjords. Quat. Sci. Rev. 89, 129–147. http://dx.doi.org/10.1016/j.quascirev.2013.12.005.

Hogg, A.G., Hua, Q., Blackwell, P.G., Niu, M., Buck, C.E., Guilderson, T.P., Heaton, T.J., Palmer, J.G., Reimer, P.J., Reimer, R.W., Turney, C.S.M., Zimmerman, S.R.H., 2013. SHCal13 Southern hemisphere calibration, 0-50,000 years cal BP. Radiocarbon 55, 655–676.

Ivy-Ochs, S., Synal, H.A., Roth, C., Schaller, M., 2004. Initial results from isotope dilution for Cl and ^{36}Cl measurements at the PSI/ETH Zurich AMS facility. Nucl. Instrum. Methods Phys. Res. Sect. B 223, 623–627.

Jomelli, V., Favier, V., Vuille, M., Braucher, R., Blard, P.-H., Khodri, M., Colose, C., Brunstein, D., Bourlès, D., Leanni, L., Rinterknecht, V., Grancher, D., Francou, B., He, F., Ceballos, J.L., Francesca, H., Liu, Z., Otto-Bliesner, B., 2014. A major advance of tropical Andean glaciers during the Antarctic Cold Reversal. Nature 513, 224–228. http://dx.doi.org/10.1038/nature13546.

Kaplan, M.R., Fogwill, C.J., Sugden, D.E., Hulton, N.R.J., Kubik, P.W., Freeman, S.P.H.T., 2008. Southern Patagonian glacial chronology for the Last Glacial period and implications for Southern Ocean climate. Quat. Sci. Rev. 27, 284–294.

Kaplan, M.R., Schaefer, J.M., Denton, G.H., Barrell, D.J.A., Chinn, T.J.H., Putnam, A.E., Doughty, A.M., 2010. Glacier retreat in New Zealand during the younger dryas stadial. Nature 467, 194–197.

Kaplan, M.R., Strelin, J.A., Schaefer, J.M., Denton, G.H., Finkel, R.C., Schwartz, R., Travis, S.G., 2011. In Situ cosmogenic ^{10}Be production rate at Lago Argentino, Patagonia: Implications for late-–glacial climate chronology. Earth Planet. Sci. Lett. 309, 21–32.

Key, R.M.A., Kozyr, C.L., Lee, S.K., Wanninkhof, R., Bullister, J.L., Feely, R.A., Millero, F.J., Mordy, C., Peng, T.-H., 2004. A global ocean carbon climatology: results from Global data Analysis Project (GLODAP). Glob. Biogeochem. Cycles 18, GB4031,. http://dx.doi.org/10.1029/2004GB002247.

Lefebre, W., Goosse, H., Timmermann, R., Fichefet, T., 2004. Influence of the southern annular mode on the sea ice ocean system. JGR 109, C09005. http://dx.doi.org/10.1029/2004JC002403.

Marshall, G.J., 2007. Half-century seasonal relationships between the Southern annular mode and Antarctic temperatures. Int. J. Climatol. 27, 373–383.

Moreno, P.I., Denton, G.H., Moreno, H., Lowell, T.V., Putnam, A.E., Kaplan, M.R., 2015. Radiocarbon chronology of the last glacial maximum and its termination in northwestern Patagonia. QSR 122, 233–249.

Mulder, T., Chapron, E., 2011. Flood deposits in continental and marine environments: character and significance. In: Slatt, R.M., Zavala, C. (Eds.), Sediment Transfert from Shelf to Deep Water-revisiting the Delivery System: AAPG Studies in Geology, vol. 61, pp. 1–30.

Phillips, F.M., Stone, W.D., Fabryka-Martin, J.T., 2001. An improved approach to calculating low-energy cosmic-ray neutron fluxes near the land/atmosphere interface. Chem. Geol. 175, 689–701.

Putnam, A.E., Denton, G.H., Schaefer, J.M., Barrell, D.J.A., Andersen, B.G., Finkel, R., Schwartz, R., Dughty, A.M., Kaplan, M., Schlüchter, C., 2010. Glacier Advance in southern middle latitudes during the Antarctic Cold reversal. Nat. Geosci. 3, 700–704.

Putnam, A.E., Schaefer, J.M., Denton, G.H., Barrell, D.J.A., Birkel, S.D., Andersen, B.G., Kaplan, M.R., Finkel, R.C., Schwartz, R., Doughty, A.M., 2013a. The Last Glacial Maximum at 44°S documented by a ^{10}Be moraine chronology at Lake Ohau, Southern Alps of NewZealand. Quat. Sci. Rev. 62, 114–141.

Putnam, A.E., Schaefer, J.M., Denton, G.H., Barrell, D.J.A., Andersen, B.G., Koffman, T.N.B., Rowan, A.V., Finkel, R.C., Rood, D.H., Schwartz, R., Vandergoesj, M.J., Plummer, M.A., Brocklehurst, S.H., Kelley, S.E., Ladig, K.L., 2013b. Warming and glacier recession in the Rakaia valley, Southern Alps of New Zealand, during Heinrich Stadial 1. Earth Planet. Sci. Lett. 382, 98–110.

Roquet, F., Park, Y.-H., Guinet, C., Bailleul, F., Charrassin, J.B., 2009. Observations of the Fawn Trough Current over the Kerguelen Plateau from instrumented elephant seals. J. Mar. Syst. 78, 377–393.

Sallée, J.B., Speer, K., Morrow, R., 2008. Response of the Antarctic circumpolar current to atmospheric variability. J. Clim. 21, 3020–3039.

Schaefer, J.M., Denton, G.H., Kaplan, M., Putnam, A., Finkel, R.C., Barrell, D.J.A., Andersen, B.G., Schwartz, R., Mackintosh, A., Chinn, T., Schlüchter, C., 2009. High-frequency holocene glacier fluctuations in New Zealand Differ from the northern signature. Science 324, 622–625.

Schimmelpfennig, I., Benedetti, L., Finkel, R., Pik, R., Blard, P.-H., Bourlès, D., Burnard, P., Williams, A., 2009. Sources of in-situ ^{36}Cl in basaltic rocks. Implic. Calibration Prod. Rates Quat. Geochronol. 6, 441–461.

Schimmelpfennig, I., Benedetti, L., Garreta, V., Pik, R., Blard, P.-H., Burnard, P., Bourles, D., Finkel, R., Ammon, K., Dunai, T., 2011. Calibration of cosmogenic ^{36}Cl production rates from Ca and K spallation in lava flows from Mt. Etna (38° N, Italy) and Payun Matru (36° S, Argentina). Geochim. Cosmochim. Acta 75, 2611–2632.

Schimmelpfennig, I., Schaefer, J.M., Akçar, N., Koffman, T., Ivy-Ochs, S., Schwartz, R., Finkel, R.C., Zimmerman, S., Schlüchter, C., 2014. A chronology of Holocene and Little Ice Age glacier culminations of the Steingletscher, Central Alps, Switzerland, based on high-sensitivity beryllium-10 moraine dating. Earth Planet. Sci. Lett. 393, 220–230.

Sharma, P., Kubik, P.W., Fehn, U., Gove, H.E., Nishiizumi, K., Elmore, D., 1990. Development of ^{36}Cl standards for AMS. Nucl. Instrum. Methods Phys. Res. Sect. B 52, 410–415.

Solomina, O., Bradley, R.S., Hodgson, D., Ivy-Ochs, S., Jomelli, V., Mackintosh, A., Nesje, A., Owen, L.A., Wanner, H., Wiles, G., Young, N.E., 2015. Holocene glacier fluctuations. QSR 111, 9–34.

Strelin, J.A., Kaplan, M.R., Vandergoes, M.J., Denton, G.H., Schaefer, J.M., 2014. Holocene glacier history of the Lago Argentino basin, Southern Patagonian Icefield. QSR 108, 124–145.

Stone, J.O., 2000. Air pressure and cosmogenic isotope production. J. Geophys. Res. 105, 23753–23759.

Stone, J.O., Fifield, K., Vasconcelos, P., 2005. Terrestrial chlorine-36 production from spallation of iron. In: Abstract of 10th International Conference on Accelerator Mass Spectrometry. September 5-10, 2005, Berkeley, USA. http://llnl.confex.com/llnl/ams10/techprogram/P1397.HTM.

St-Onge, G., Chapron, E., Mulsow, S., Salas, M., Viel, M., Debret, M., Foucher, A., Mulder, T., Winiarski, T., Desmet, M., Costa, P.J.M., Ghaleb, B., Jaouen, A., Locat, J., 2012. Comparison of earthquake-triggered turbidites from the Saguenay (Eastern Canada) and Reloncavi (Chilean margin) Fjords: implications for paleoseismicity and sedimentology. Sediment. Geol. 243–244, 89–107.

Syvitski, J.P., 1991. Towards an understanding of sediment deposition on glaciated continental shelves. Cont. Shelf Res. 11, 897–937.

Thompson, D.W.L., Wallace, J.M., 2000. Annular modes in the extratropical circulation. Part 1: Month to month variability. J. Clim. 13, 1000–1016.

Thompson, D.W.J., Solomon, S., Kushner, P.J., England, M.H., Grise, K.M., Karoly, D.J.,

2011. Signatures of the Antarctic ozone hole in Southern Hemisphere surface climate change. Nat. Geosci. 4, 741–749.
Van der Putten, N., Verbruggen, C., Björck, S., Michel, E., Disnar, J.-R., Chapron, E., Moine, B.N., de Beaulieu, J.-L., 2015. The last termination in the South Indian Ocean: A unique terrestrial record from Kerguelen Islands (49°S) situated with the Southern Hemisphere westerly belt. Quat. Sci. Rev. 122, 142–157.
Van Rensbergen, P., de Batist, M., Beck, C., Chapron, E., 1999. High-resolution seismic stratigraphy of glacial to interglacial fill of a deep glacigenic lake: Lake Le Bourget, Northwestern Alps, France. Sediment. Geol. 128, 99–129.
Vasskog, K., Nesje, A., Storen, E.N., Waldmann, N., Chapron, E., Ariztegui, D., 2011. A Holocene record of snow-avalanche and flood activity reconstructed from a lacustrine sedimentary sequence in Oldevatnet, western Norway. Holocene 21 (4), 597–614.
Viel, M., Chapron, E., Mulsow, S., Desmet, M., Winiarski, T., Debret, M., 2015. Evidencia de la actividad paleosismica y caracterizacion de los porcesos sedimentarios en la Cuenca subacuatica de Reloncavi, Norpatagonia, Chile. Cienc. Tecnol. Mar. 36, 9–34.
Verfaillie, D., Favier, V., Dumont, D., Jomelli, V., Gilbert, A., Brunstein, D., Gallée, H., Frenot, Y., 2015. Recent glacier decline in the Kerguelen Islands (49°S, 69°E) derived from modeling, field observations, and satellite data. JGR 120, 637–654.
WAIS divide Project Members, 2013. Onset of deglaciation warming in west Antarctica driven by local orbital forcing. Nature 500, 440–446.